Final Report

NASA Cooperative Agreement NCC2-450

covering the period

January, 1987 - January, 1989

Principal Investigator - Jon A. Hoffmann

The Influence of Free-Stream Turbulence on Turbulent Boundary Layers with Mild Adverse Pressure Gradients

by

J. A. Hoffmann, Professor
S. M. Kassir, Graduate Student
S. M. Larwood, Student Assistant

November, 1988

Aeronautical Engineering Department
California Polytechnic State University
San Luis Obispo, California

Abstract

The influence of near isotropic free-stream turbulence on the shape factors and skin friction coefficients of turbulent boundary layers is presented for the cases of zero and mild adverse pressure gradients. With free-stream turbulence, improved fluid mixing occurs in boundary layers with adverse pressure gradients relative to the zero pressure gradient condition, with the same free-stream turbulence intensity and length scale. Stronger boundary layers with lower shape factors occur as a result of a lower ratio of the integral scale of turbulence to the boundary layer thickness, and to vortex stretching of the turbulent eddies in the free-stream, both of which act to improve the transmission of momentum from the free-stream to the boundary layers.

Nomenclature

A, B, D	Constants for turbulence decay, dissipation length scale and autocorrelation coefficient equations
c_f	Boundary layer skin friction coefficient
Δc_f, ΔH	Change in c_f and H with free-stream turbulence compared to the low free-stream turbulence condition at the same α, Re_θ and dP/dx.
C_p	Static pressure coefficient along plate, $= P(x)-P(x=0.56m)/\rho(U_\infty(x=0.56m))^2/2$
d	Diameter
E	Time averaged dc voltage output of the hot wire anemometer system
$\sqrt{e'^2}$	Time averaged rms voltage output of the hot wire anemometer system
H	Boundary layer shape factor, $= \delta^*/\theta$
K	Constant, $= c_{f_o}$(experimental)/c_{f_o}(empirical)
L_x	Dissipation length scale
LFST	Low free-stream turbulence
M	Mesh size of turbulence generators
n, m, k	Exponents for turbulence decay, dissipation length scale and autocorrelation coefficient equations
P	Static pressure
$\sqrt{q'^2}$	Total rms free-stream turbulence fluctuation, $= \sqrt{(\overline{u'^2} + \overline{v'^2} + \overline{w'^2})/3}$
R_x	Free-stream Autocorrelation coefficient, $= \overline{u'(t)\, u'(t-\Delta t)}/\overline{u'^2}$
Re_θ	Reynolds number based on θ, $= U_\infty\theta/\nu$
t	time
u', v', w'	Free-stream velocity fluctuations in the x, y and z directions respectively
U_∞	Free-stream time averaged velocity

$\bar{u}$	Time averaged velocity
u_*	Shear velocity
x,y,z	Coordinate system relative to leading edge of flat plate
x', y'	Coordinate system relative to rods
X_o	Distance from rods to leading edge of flat plate
α	Angle of incidence of flat plate relative to the zero pressure gradient case.
β	Pressure gradient parameter, $= (\delta^*/\tau_o)/(dP/dx)$
λ_x	Integral length scale of turbulence, $= \int_o^\infty R_x \, dx$
δ, δ^*, θ	Boundary layer thickness when $\bar{u} = 0.995\ U_\infty$, displacement thickness and momentum thickness respectively.
Θ	Divergence angle of diffuser wall
ν	Kinematic viscosity
τ_o	Wall shear stress
ρ	Fluid density
Π	Wake parameter

SUBSCRIPTS

o	Low free-stream turbulence condition
MAX	Maximum

Table of Contents

List of Figures

Introduction

Although many turbulent boundary layers encountered in engineering experience a turbulent flow above them, little information is available for designers which can be used to predict the effects that external turbulence will have on the boundary layers. Examples of flows with turbulent boundary layers under external turbulence or flows in which a boundary layer encounters the turbulent wake of a preceding object include turbomachinery blading, ejectors, airfoils downstream of a propeller or canard, as well as a wide variety of other internal and external flows where upstream free-stream turbulence exists. Also in nature, it is observed that fish swim in schools and birds fly in formation.

Available literature has addressed the effects of isotropic homogeneous free-stream turbulence on the shape parameters of turbulent boundary layers with a zero pressure gradient. An investigation by Raghunathan (1) showed that the skin friction coefficient (c_f) and the boundary layers thickness (δ) increased, and the shape factor (H) decreased with increasing free-stream turbulence intensity ($\sqrt{u'^2}/U_\infty$). Hancock (2) extended this result to incorporate the effect of the free-stream dissipation length scale (L_x), and found that c_f and δ increased and H decreased when increasing a free-stream turbulence parameter defined as $(\sqrt{u'^2}/U_\infty)/(L_x/\delta + 2)$. Castro (3) found that Hancock's results were Reynolds number dependent for $Re_\theta < 2{,}000$.

The turbulent structure of a turbulent boundary layer, for the case of a zero pressure gradient, has been found to be affected by free-stream turbulence. An investigation by Huffman (4) for the case of isotropic free-stream turbulence found that the Reynolds stress and turbulent kinetic energy in the outer part of the boundary layer ($y/\delta>0.4$) increased as the free-stream turbulence intensity ($\sqrt{u'^2}/U_\infty$) increased, and that these parameters were essentially independent of ($\sqrt{u'^2}/U_\infty$) for $y/\delta<0.4$. An investigation by Fang (5) for the case of near isotropic ($\sqrt{v'^2}/\sqrt{u'^2}\approx1$) and highly anisotropic free-stream turbulence ($\sqrt{v'^2}/\sqrt{u'^2} > 2.5$) with a turbulent boundary layer in a near zero pressure gradient showed that the highly anisotropic free-stream turbulence condition results in larger isotropy ($\sqrt{v'^2}/\sqrt{u'^2} >1$) in the outer part of the boundary layer ($y/\delta > 0.6$), and found that $\sqrt{v'^2}/\sqrt{u'^2} \approx 1$ for the case of near isotropic free-stream turbulence when $y/\delta > 0.6$; for the case of a conventional turbulent boundary layer without free-stream turbulence,

$\sqrt{\overline{v'^2}}/\sqrt{\overline{u'^2}} < 1$ for all y/δ. The larger values of the Reynolds stresses, turbulent kinetic energy and isotropy ratios that exist in the outer part of boundary layers under free-stream turbulence, as reported by Huffman and Fang, are apparently factors which promote improved mixing and correspondingly decrease the shape factors of boundary layers relative to the low free-stream turbulence condition.

The effects of free-stream turbulence on the shape parameters and the structure of turbulent boundary layers with adverse pressure gradients has been evaluated by Arnal (17). Significant improvements in boundary layer strength were obtained when free-stream turbulence and adverse pressure gradients were coupled, resulting in a delay of separation which would otherwise occur without free-stream turbulence.

The effects of near-isotropic and highly anisotropic inlet free-stream turbulence on the performance of a two-dimensional diffuser, an internal flow with an adverse pressure gradient, has been studied by Hoffmann (6)(7)(8). Improvements in the pressure recovery coefficient of the diffuser (C_p) of approximately 10% at a total included divergence angle (2Θ) of 12° (near peak C_p) and 24% at $2\Theta = 20°$ (in the large transitory stall regime) were obtained. These improvements in C_p can be attained with a low turbulence generator total pressure loss; it was found that the ratio of the increase in C_p to the dimensionless total pressure loss of the turbulence generator could be larger than 13(8). These high gains in C_p were attained with high inlet total free-stream turbulence intensities ($\sqrt{\overline{q'^2}}/U_\infty > 3.5\%$), high free-stream isotropy ratios ($\sqrt{\overline{v'^2}}/\sqrt{\overline{u'^2}} > 2.1$), and with the axes of the turbulence generators aligned so that the axes of the turbulent eddies are parallel to the diverging walls of the diffuser and perpendicular to the flow. It was also found that isotropic inlet free-stream turbulence can be significantly less effective at improving C_p as compared to highly anisotropic inlet free-stream turbulence (8). The increases in C_p were shown to be a result of both delayed separation and reduced distortion within the diffuser (7).

In this study, the effects of free-stream turbulence on established turbulent boundary layers are evaluated. Free-stream turbulence can also alter the position of boundary layer transition; one recent paper on this topic is presented by Meier (14).

Generally, the most critical stage for a boundary layers development is encountered when it experiences a decelerating external free-stream flow and a corresponding adverse pressure gradient. For the case of boundary layers under low free-stream turbulence, this adverse pressure gradient can weaken the boundary layer (exhibited by an increase in the shape factor (H)) which may eventually lead to flow separation and a corresponding loss of pressure for internal flows, or a loss of lift and increase in drag for external flows. It is the purpose of this study to evaluate the effects of free-stream turbulence on turbulent boundary layers with mild adverse pressure gradients. The results will then be available for use by designers for both internal and external flows with free-stream turbulence.

Experimental System & Procedure

To evaluate the effects of free-stream turbulence on turbulent boundary layers, a flat plate was positioned in a wind tunnel and a set of rods was positioned upstream of the plate to generate free-stream turbulence. A detailed description of the system and instrumentation follows.

All experiments were performed in the Cal Poly draw-thru wind tunnel, illustrated in Fig. 1. The test section has cross-sectional dimensions of 0.88 mx 1.18 m. Screens and honeycomb upstream of the contraction, and a contraction ratio of 10:1, provide a relatively low turbulence intensity ($\sqrt{u'^2}/U_\infty$ = 0.25%) at the test section. All experiments were performed holding the velocity upstream of the rods constant at 24.1 m/s.

A set of monoplane parallel rods which span the entire cross-section of the test section of the wind tunnel with a solidity (d/M) of 0.32 and M = 6.67 cm. (see Fig. 2) was positioned at two locations upstream of the leading edge of the flat plate (X_o = 0.67 m and X_o = 1.13 m).

The flat plate which spans the entire height of the test section of the wind tunnel as shown in Fig. 2 was constructed from 1.90 cm plywood, and was varnished and sanded to obtain a smooth surface. The plate pivots near the center (x = 0.63 m) to obtain various angles of incidence to the free-stream flow. The distance from the tunnel wall to the surface of the flat plate at the location of the pivot is 0.32 m. Experimentation was performed at three different angles of incidence. The plate was first positioned to obtain a zero static pressure gradient - the α = 0° position; for α = 0°, the plate and tunnel wall formed a diffuser with a 1.5° total included divergence angle. The plate was then adjusted to obtain adverse pressure gradients with α = 2.6° and α = 5.2°, inclined from the α = 0° position. The leading edge of the plate has a 2.5 cm radius; it was found that leading edge separation occurred at α = 2.6° and 5.2° when a 0.95 cm radius was used. Masking tape was applied to the leading edge of the plate, which tripped the boundary layer; leading edge separation also occurred at α = 2.6° and α = 5.2° when masking tape was not attached.

The flat plate has six equally spaced static pressure taps located near the center line of the plate beginning at x = 0.30 m; at two of these x locations (x = 0.56m and x = 0.94 m), the plate is instrumented with two Preston tubes of different diameter (d = 0.52mm and d = 0.82mm) and four fixed

total pressure probes with d = 0.82 mm located at various y positions used to determine velocities near the surface. The measured velocities near the surface fit the logarithmic law of the wall formula, equation 4, and were used to obtain u_* and c_f for all test conditions. In order to determine velocities above the plate at any y position, a total pressure probe (d = 0.82 mm) was attached to a remote-controlled model B2509WIJ Velmex Inc. electric traversing mechanism. The voltage output of the mechanism, proportional to y, was measured using a HP model 3466A digital multimeter. The velocity pressure at each location was fed into a Celesco Model P15D± 0.1PSID pressure transducer, and then through a Model CD 10 Carrier Demodulator into a TSI model 1076 multimeter, to obtain a ten second time average of the velocity pressure. A cubic spline curve fit of the velocity pressures and velocities was obtained, using a computer program, resulting in values of δ, δ^*, θ and H for the boundary layers.

Free-stream turbulence intensity and velocity traverses downstream of the rods were obtained using a TSI model 1050 anemometer and a TSI model 1052 linearizer. The average voltage output of the linearizer (E) from a single wire normal to the mean flow, proportional to average velocity, was averaged for a 10 second period of time using a TSI model 1076 voltmeter, and the rms voltage output ($\sqrt{e'^2}$) was averaged for a two second period of time using a HP model 3400A true rms meter. The probe was attached to a remote-controlled model B2509W1J Velmex Inc. electric traversing mechanism which produced a voltage output proportional to distance. These three voltages were fed into a HP model 1090A plotter to generate the velocity and turbulence vs. distance graphs in the non-homogenous flow region downstream of the rods.

Free-stream turbulence measurements were obtained at two streamwise locations above the flat plate (x = 0.56 m and x = 0.94 m) using single wires normal to the flow and a wire inclined at 45° to the flow. The output of a single wire normal to the flow was also fed into a model 2032 B and K wave analyzer to generate plots of the autocorrelation coefficient vs. Δt. For these measurements, a TSI model 1057 signal conditioner was used after the linearizer, using a 50 kHz low pass filter to eliminate the noise of the anemometer and a 50 Hz high pass filter so that the values of R_x more rapidly approach zero at large Δt, which thereby facilitated λ_x to be calculated more easily. The average decrease in the measured turbulence intensity ($\sqrt{u'^2}/U_\infty$) due to the use of the high pass filter was 3.2%; no measurable difference

occurred due to the use of the low pass filter. Equations of the form $R_x = De^{k\Delta t}$, each valid for a given range of Δt, were obtained and these equations were then mathematically integrated to obtain the area under the curve and, correspondingly, the integral scale of turbulence.

Results and Discussion

I) Free-Stream Flow Field Downstream of Rods

The free-stream flow field downstream of the rods was first measured without the flat plate installed in the wind tunnel. For this condition, a small favorable pressure gradient exists due to boundary layer growth on the walls of the constant area test section. The average rms and dc voltage outputs of the linearizer of the hot wire anemometer system were obtained at several locations downstream of the rods, $0.38 \leq x'/M \leq 7.90$, for $0.27 \leq y'/M \leq 2.25$ and are presented in Figs. 3 thru 8. The x'-y' axis is located at the center of the fourth rod from the tunnel wall (see Fig. 2). The average approach velocity for each traverse was 24.1 m/s. For $x'/M < 7.9$, the peak dc voltage output and the minimum rms voltage outputs of the hot wire, which occurs for flow between the rods, are directly proportional to $\bar{u}$ and $\sqrt{\overline{u'^2}}$ respectively, whereas the voltage outputs at the other y' locations represent velocity and turbulence levels in the x'- y' plane. A small difference in the location of the peak velocity and the minimum turbulence intensity occurs for each traverse. This difference is attributable to the 10 second time average used to obtain E and the two second time average used to obtain $\sqrt{\overline{e'^2}}$.

A plot representing the nonuniformity of the flow in the nonhomogeneous flow region downstream of the rods is presented in Fig. 9. Extrapolation of the plot shows that the variation of u as a function of y' is less than 1% for $x'/M > 8$ or $x' > 0.53$m. In the region of essentially homogeneous flow downstream of the rods, turbulence decay was represented by equation 1; values of A and n are presented in table 1.

$$\overline{u'^2}/U_\infty^2 = A\, x'^n \qquad \text{Eqn. 1}$$

Now that the region with essentially homogeneous flow has been identified as $x' > 0.53$m, the flat plate was installed in the wind tunnel with its leading edge positioned in the homogeneous flow region downstream of the rods (X_o = 0.67m and 1.13m), and with α = 0°, 2.6° and 5.2° to obtain a zero pressure gradient and two conditions with mild adverse pressure gradients. Curves of the static pressure coefficient of the plate (this static pressure coefficient is based on the measured static pressure and free-stream velocity at x = 0.56 m) vs. x are presented in Fig. 10. The results show that the dimensionless static pressure gradient along the plate is essentially unaffected by the free-stream turbulence conditions and boundary layer growth

at each α, and is a weak function of x. A dimensionless pressure gradient parameter (β) representing a ratio of the pressure forces to the shear forces in a section of the boundary layer (15) is presented in Table 2 and was not held constant in this study; dP/dx was calculated using a potential flow solution and the measured free-stream velocities at x = 0.56 m and x = 0.94 m. The turbulence measurements, presented in Table 2, show a near isotropic free-stream flow. For the case of $\alpha = 0°$, the turbulence decay and the dissipation length scale equations (equations 1 and 2) were used to obtain the free-stream dissipation length scale (L_x) as shown in equation 3. Values of A, B, n and m are presented in Table 1, and values of L_x for each test condition at $\alpha = 0°$ are presented in Table 2.

$$U_\infty d(\overline{u'^2})/dx' = -(\overline{u'^2})^{3/2}/L_x \qquad \text{Eqn. 2}$$

$$L_x = B\, x'^m \qquad \text{Eqn. 3}$$

The rate of turbulence decay - or the value of n in equation 1, has been found to be a function of the geometry, the solidity, and the distance downstream of the turbulence generator. For the zero pressure gradient condition, the values of A and n are listed in Table 1 and show that n increases as x' increases.

Free-stream integral length scales (λ_x) were obtained by finding the area under the R_x vs. Δt curves; a sample curve from the wave analyzer presented in Fig. 11, shows a smooth curve representative of a broad-band turbulence. The results, presented in Table 2 and Fig. 12, show an increase in eddy size with downstream distance, and a decrease in eddy size with increasing α at any x'. The results indicate that vortex stretching occurs in the y direction due to diffusion in the y direction, which results in the lower measured values of λ_x at $\alpha = 2.6°$ and 5.2°, relative to $\alpha = 0°$.

II) Turbulent Boundary Layer Results

The influence of free-stream turbulence on turbulent boundary layers is described below. The velocity profiles with different free-stream turbulence conditions and angles of plate incidence were the base boundary layer data obtained from which values of c_f, δ and H were obtained. The results are presented in Table 2. As shown in Fig. 13, the velocity profiles near the wall fit the logarithmic zone law of the wall formula well (equation 4), demonstrating that neither the free-stream turbulence levels nor the adverse

pressure gradients encountered in this study affect this relationship. The velocity profiles in the outer regions of the boundary layers have been related to a wake parameter, which has been shown to be dependent upon β and a free-stream turbulence parameter (see the appendix).

$$\bar{u}/u_* = 2.439 \ln u_* y/\nu + 5.2 \qquad \text{Eqn. 4}$$

A) Values of c_{fo} and H_o

To evaluate the effects of free-stream turbulence on turbulent boundary layers, all values of c_f and H for conditions with free-stream turbulence were compared to values of c_{fo} and H_o (values of c_f and H with low free-stream turbulence) holding Re_θ, α and dP/dx constant. Values of c_f and H, with and without free-stream turbulence, were compared at the same x locations at each α, where essentially the same values of dP/dx (or the same values of U_∞ and dU_∞/dx) exist. The data obtained resulted in different Re_θ for boundary layers with and without free-stream turbulence at each x and α (as much as 10% difference occurred). Empirical formulas which fit the data of c_{fo} and H_o at each value of x and α were used to obtain values of c_{fo} and H_o at the Re_θ corresponding to each condition with free-stream turbulence.

Values of H_o at each α and x were obtained by numerical integration of formulas developed by von Doenhoff and Tetervin (9), equation 5 and 6. The division of equation 6 by equation 5, with U_∞ and dU_∞/dx held constant, presents a relationship for $H_o = f(\theta)$. The original work by von-Doenhoff and Tetervin ignored the effect of dP/dx on c_f. Equation 6, presented by Hirst (10) uses the Ludwieg and Tillman formula (11) (equation 7 with K=1) and thereby incorporates the effect of dP/dx on c_f.

$$d\theta/dx = c_{fo}/2 - (H_o+2)(\theta/U_\infty)\, dU_\infty/dx \qquad \text{Eqn. 5}$$

$$dH_o/dx = e^{4.68(H_o - 2.975)} \left[-(2/U_\infty)(dU_\infty/dx)[5.89 \log 4.075 Re_\theta]^2 - 2.035(H_o-1.286)/\theta\right] \qquad \text{Eqn. 6}$$

$$c_{fo} = 0.246K / 10^{0.678 H_o Re_\theta^{0.268}} \qquad \text{Eqn. 7}$$

In the use of equations 5 and 6, the initial conditions used were the values of H_o, θ and c_{fo} obtained at each x and α with low free-stream

turbulence. Values of dU_∞/dx were obtained from a potential flow solution using measured free-stream velocities at both x = 0.56 m and x = 0.94 m at each α. The maximum percentage change in H_o due to this extrapolation, for the range of Re_θ encountered in the tests with free-stream turbulence, was 0.6%.

Curves of $H_o = f(Re_\theta)$ were also obtained from equation 5 and 6, integrating with respect to x. The potential flow solution was used which presents U_∞ and $dU_\infty/dx = f(x)$. Curves which best fit the measured values of H_o and θ at x = 0.56m and x = 0.94m at each α are presented in Fig. 14. All measured values of H_o fit these formulas within ± 1.5%.

Values of c_{f_o} corresponding to the Re_θ with free-stream turbulence for $\alpha = 0°$ at each x were obtained using a modified Clauser's formula (12), equation 8, and values of c_{f_o} for $\alpha = 2.6°$ and 5.2° at each dP/dx were obtained using a modified Ludwieg and Tillman formula (11), equation 7. In these equations, values of H_o were obtained from the von Doenhoff and Tetervin formulas.

$$c_{f_o} = K/(3.96 \log H_o Re_\theta + 3.04)^2 \qquad \text{Eqn. 8}$$

The value of K is an indicator of the magnitude of the departure of the results of this study from results with K = 1 as obtained by Clauser, and Ludwieg and Tillman. As shown in Table 2a, the maximum departure obtained was 5%. The maximum precentage change in c_{f_o} due to this extrapolation, for the range of Re_θ encountered in the tests with free-stream turbulence, was 1.3%.

Curves of $c_{f_o} = f(Re_\theta)$ which best fit the data at both x = 0.56m and x = 0.94m were obtained using equation 8 for $\alpha = 0°$ and equation 7 for $\alpha = 2.6°$ and 5.2°. The results are presented in Fig. 15. All measured values of c_{f_o} fit these formulas within ± 1.6%.

The magnitudes of H_o and c_{f_o} at each α, as shown in Figs. 14 and 15, are affected by different initial conditions for the boundary layers which occur at each α. It is observed that the value of H_o at x = 0.56m and $\alpha = 5.2°$ is lower compared to the value at x = 0.56m and $\alpha = 2.6°$, and the trend of c_{f_o} at $\alpha = 5.2°$ appears high relative to that at $\alpha = 2.6°$. Larger values of U_∞ over the plate occur as α increases due to blockage caused by the plate in the test section; it is concluded that this flow acceleration results in lower values of H_o and larger values of c_{f_o} near the leading edge of the plate with

increasing α, as compared to the values that would occur without plate blockage. In this study, the boundary layers with free-stream turbulence are compared to those without free-stream turbulence at the same values of α (as well as x and Re_θ) and therefore with essentially the same free-stream velocity distribution.

B) Zero Pressure Gradient Case with Free-Stream Turbulence.

For the conditions with free-stream turbulence and a zero pressure gradient, the results of this study are compared to those of Hancock (2). A comparison of values of $\Delta c_f/c_{fo}$ at various values of $\sqrt{u'^2}/U_\infty/(L_x/\delta + 2)$ is presented in Fig. 16 and the relationship between $\Delta c_f/c_{fo}$ and $\Delta H/Ho$ is presented in Fig. 17. The results of this study agree reasonably well with those of Hancock (2), considering differences in the experimental system used by both investigators (e.g. Hancock used a flat plate with a sharp leading edge, while a rounded leading edge with some flow acceleration after the rods due to plate blockage was used in this study) and the repeatability of the results of both investigations.

C) Adverse Pressure Gradient Case with Free-Stream Turbulence.

Curves of H vs. Re_θ for $\alpha = 0°$, 2.6° and 5.2° are presented in Fig. 14. For the case with free-stream turbulence, relatively low values of H occur for $\alpha = 2.6°$ and $\alpha = 5.2°$ compared to $\alpha = 0°$ for constant $\sqrt{q'^2}/U_\infty$; values of H at $\alpha = 2.6°$ and $\alpha = 5.2°$ appear to be relatively independent of Re_θ for constant $\sqrt{q'^2}/U_\infty$. Traditionally for the case without free-stream turbulence, an increase in H is expected with increasing Re_θ, and the rate of increase of H should increase as α increases, as shown on Fig. 14 for the cases without free-stream turbulence. Curves of c_f vs. Re_θ shown in Fig. 15 also show large magnitudes of c_f for conditions with free-stream turbulence at all α, relative to the values of c_{fo}. An explanation for these remarkable improvements in boundary layer strength is addressed below.

In Fig. 18, values of $\Delta H/H_o$ are plotted as a function of a free-stream turbulence parameter, $\sqrt{q'^2}/U_\infty/\lambda_x/\delta$, based on the integral length scale. This parameter, which places a larger weight on the free-stream length scale, is somewhat different than the free-stream turbulence parameter used by Hancock, $\sqrt{u'^2}/U_\infty$ $/(L_x/\delta + 2)$, which is based on the dissipation length scale. In Fig. 18, it can be seen that a best fit curve for $\alpha = 0°$ exists, and a separate best fit curve for both $\alpha = 2.6°$ and $\alpha = 5.2°$ exists. As shown in Fig. 19, the data for $\Delta c_f/c_{fo}$ is again generally lower for $\alpha = 0°$, relative to the data

for both $\alpha = 2.6°$ and $\alpha = 5.2°$. With $\sqrt{\overline{q'^2}}/U_\infty/\lambda_x/\delta = 2.1$, values of $\Delta H/H_o$ and $\Delta c_f/c_{fo}$ at $\alpha = 2.6°$ are both about 25% larger compared to those at $\alpha = 0°$.

As a result of a higher repeatability of $\Delta c_f/c_{fo}$ relative to $\Delta H/H_o$, more distinction of the results of this study can be obtained by evaluating the data of $\Delta c_f/c_{fo}$. An inspection of Fig. 19 shows that at $\alpha = 0°$, values of $\Delta c_f/c_{fo}$ appear to be independent of Re_θ for $2500<Re_\theta<3900$. Castro (3) found that for $\alpha = 0°$, values of $\Delta c_f/c_{fo}$ were independent of Re_θ for $Re_\theta>2000$. The single curve presented for $\alpha = 2.6°$ and $\alpha = 5.2°$ appears to be applicable for $Re_\theta \simeq 5000$ when $\alpha = 2.6°$ and for $Re_\theta \simeq 9000$ when $\alpha = 5.2°$; the results at lower Re_θ with $\alpha = 5.2°$ fall below this curve. More data with a larger range of Re_θ needs to be obtained to better define the limitations of this preliminary study.

The results presented suggest that an improvement in fluid mixing occurs for both $\alpha = 2.6°$ and $\alpha = 5.2°$, relative to $\alpha = 0°$. Two major differences occur with boundary layers under free-stream turbulence with adverse pressure gradients relative to the zero pressure gradient condition. First, the boundary layer thickness is larger for the adverse pressure gradient condition relative to the zero pressure gradient condition. For the same free-stream length scale, values of λ_x/δ are smaller resulting in more effective mixing. Hancock (2) has also shown that lower values of L_x/δ result in larger values of $\Delta H/H_o$ and $\Delta c_f/c_{fo}$ for the condition of $\alpha = 0°$ with the same $\sqrt{\overline{q'^2}}/U_\infty$. Since the free-stream turbulence parameter reflects changes in both $\sqrt{\overline{q'^2}}/U_\infty$ and λ_x/δ, one would expect that another fluid mechanism exists which causes the larger values of $\Delta H/H_o$ and $\Delta c_f/c_{fo}$ at constant $\sqrt{\overline{q'^2}}/U_\infty/\lambda x/\delta$ with adverse pressure gradients relative to the zero pressure gradient condition. Second, for the case of boundary layers with an adverse pressure gradient, vortex stretching of the turbulent eddies in the free-stream occurs in the y direction as a result of diffusion of the flow in the y direction; this is reflected by a decrease in λ_x with increasing α as shown in Fig. 12. It is concluded that the effectiveness of fluid mixing is augmented for conditions with adverse pressure gradients and with free-stream turbulence, due to vortex stretching and an associated increase in vorticity of the eddies. In another study, Viets (13) investigated the effect of vortex stretching within the boundary layer for flow in a diffuser with low free-stream inlet turbulence. He found that diffusion normal to the plane of the velocity profile leads to improved mixing in contrast to diffusion in the plane of the velocity profile.

For this study, improved mixing occurs with free-stream turbulence and diffusion in the plane of the velocity profile. The work of Arnal (17) has also revealed that increases in boundary layer strength can occur when free-stream turbulence and adverse pressure gradients are coupled; the work presented in this paper identifies, for the first time, the fluid mechanisms responsible for this improvement in boundary layer strength. In Arnal's experiment with a large adverse pressure gradient and a boundary layer near separation for the low free-stream turbulence condition, relatively large fractional changes in H and c_f were obtained ($\Delta H/H_o \simeq 0.25$ and $\Delta c_f/c_{fo} \simeq 5$) when $\sqrt{\overline{q'^2}}/U_\infty$ was approximately 5%. A direct comparison of the results of Arnal with the results presented in this paper is made difficult due to the lack of λ_x data in Arnal's work.

A plot of $\Delta c_f/c_{fo}$ vs. $\Delta H/H_o$, presented in Fig. 17, shows that for the same incremental change in $\Delta c_f/c_{fo}$ lower values of $\Delta H/H_o$ generally occur for $\alpha = 2.6°$ and $\alpha = 5.2°$, relative to Hancock's results for $\alpha = 0°$. The two data points on the left of Hancock's curve occur for low Re_θ for the respective values of α; Castro (3) also obtained data on the left of Hancock's curve for low Re_θ with $\alpha = 0°$. Castro (3) also obtained data on the left of Hancock's curve for low Re_θ with $\alpha = 0°$.

III) Accuracy and Repeatability

In this study, values of H and c_f are related to a free-stream turbulence parameter, $\sqrt{\overline{q'^2}}/U_\infty/\lambda_x/\delta$. Values of H and c_f were both found to be repeatable within ± 1.5%, with 20:1 odds. As a result of the relatively small values of Δc_f and ΔH, the repeatability of $\Delta c_f/c_{fo}$ is ± 0.02, or ± 10% with $\Delta c_f/c_{fo} = 0.2$. The repeatability of $\Delta H/H_o$ is ± 0.02, or ± 20% if $\Delta H/H_o$ is 0.1. Actual magnitudes of c_f for the condition of low free-stream turbulence were found to differ from those of other investigation by as much as 5%, probably due to differences in experimental systems. Values of the free-stream turbulence parameter were found to be repeatable within ± 10%.

Conclusions

Traditionally, adverse pressure gradients have been considered a menace to the boundary layer which can weaken it and eventually lead to flow separation. Indeed, this is true for the case of a boundary layer with low free-stream turbulence. The results of this study have shown that, for the case of turbulent boundary layers under external free-stream turbulence, improved mixing and a more effective transmission of momentum from the free-stream to the boundary layer occurs when mild adverse pressure gradients exist, relative to the zero pressure gradient case with the same values of the free-stream total turbulence intensity and integral length scale. The boundary layer shape factor has been shown to remain constant, within the limits of the uncertainity of the data, with increasing Re_θ. The fluid mechanisms responsible for this improved mixing and corresponding stronger boundary layers with lower shape factors are:

1) A reduction of the ratio of the free-stream integral scale of turbulence to the boundary layer thickness (λ_x/δ) generally occurs with boundary layers in adverse pressure gradient flow fields. This reduction in λ_x/δ is primarily due to the increase in δ which naturally occurs when adverse pressure gradients exist, relative to smaller values of δ which occur for the zero pressure gradient case.

2) Vortex stretching of the turbulent eddies in the free-stream occurs when adverse pressure gradients exist, resulting in a higher vorticity and a corresponding augmentation of fluid mixing.

In this manuscript, values of the fractional changes in H and c_f that occur with free-stream turbulence relative to the values without free-stream turbulence, are presented as a function of a free-stream turbulence parameter, $\sqrt{q'^2}/U_\infty/\lambda_x/\delta$, for conditions with zero and mild adverse pressure gradients. The changes in c_f and H obtained appear to be dependent upon Re_θ for low Re_θ. For this preliminary study, values of λ_x/δ were on the order of magnitude of 1. Intuitively, one would expect that the free-stream would not exert as much effect on the boundary layer for very small values if λ_x/δ; for very large values of λ_x/δ, an unsteady boundary layer would be expected. Future studies should investigate the effect of free-stream turbulence on boundary layers with favorable pressure gradients, as well as boundary layers with high adverse pressure gradients, using a larger range of free-stream turbulence

conditions as well as a larger range of Re_θ. Now that the fluid mechanisms resulting in improved boundary layer strength have been identified, mathematical modeling can begin to predict boundary layer parameters for a wide variety of flow conditions with free-stream turbulence.

Acknowledgements

The authors gratefully acknowledge the sponsorship of this project by NASA-ARC through grant #NCC 2-450. Student assistants who meticulously worked on various phases of the project include Ben Arbogast, Chuck Brands, Trong Bui, Benson Chan, Joan Goetz, Jeff Joseph, Heather Miller, Tom Obert, Ted Oehinger, Lee Peron, Pat Pielage, Matt Poff, Francis Pugh, Bill Scott, Bruce Storms, Neil Swanson, Duc Tran and Liza Won.

BIBLIOGRAPHY

1. Raghuanthan, S. and McAdam, R. J. W., "Free-Stream Turbulence Effects on Attached Subsonic Turbulent Boundary Layer." AIAA Journal, Vol. 21, No. 4, 1983.

2. Hancock, P. E. and Bradshaw, P., "The Effect of Free-Stream Turbulence on Turbulent Boundary Layers." ASME Journal of Fluids Engineering, Vol. 105, September 1983, p. 284.

3. Castro, I. P., "Effects of Free-Stream Turbulence on Low Reynolds Number Boundary Layers." ASME Journal of Fluids Engineering, Vol. 106, September 1984.

4. Huffman, G. D., Zimmerman, D. R. and Bennett, W. A., "The Effect of Free-Stream Turbulence Level on Turbulent Boundary Layer Behavior." AGARD, No. 164 on Boundary Layer Effects in Turbomachines, edited by J. Surugus, April, 1972.

5. Fang, Liang-Wei and Hoffmann, Jon A., "The Effects of Anisotropic Free-Stream Turbulence on Turbulent Boundary Layer Behavior," NASA-CR-177379, November, 1985.

6. Hoffmann, J. A., "Effects of Free-Stream Turbulence on Diffuser Performance." ASME Journal of Fluids Engineering, Vol. 103, September, 1981, pp. 385-390.

7. Hoffmann, J. A. and Gonzalez, G., "Effects of Small Scale, High Intensity Inlet Turbulence on Flow in Two Dimensional Diffuser." ASME Journal of Fluids Engineering, Vol. 106, June, 1984, pp. 121-124.

8. Hoffmann, Jon A. and Fang, Liang-Wei "Observations of the Structure of Inlet Free-Stream Turbulence on Diffuser Performance," AIAA Paper 88-3673-CP, presented at The First National Fluid Dynamics Congress, July 24-28, 1988.

9. Doenhoff, A. E., and N. Tetervin, "Determination of General Relations for the Behavior of Turbulent Boundary Layers," Nat. Advisory Comm. Aeron., Rept. 772 (1943).

10. Hurst, E. A. and Reynolds, W. C., "An Integral Prediction Method for Turbulent Boundary Layers Using the Turbulent Kinetic Equation," Rept. MD-21, Thermosciences Division, Stanford University, June, 1968.

11. Ludwieg, H., and W. Tillman, "Investigations of the Wall-Shearing Stress in Turbulent Boundary Layers," Nat. Advisory Comm. Aeron., Tech. Memo. 1285 (1950); Transl. from Z. Angew. Math. Mech., 29 (1949).

12. Harleman, D. R. F. and Daily, J. W., Fluid Dynamics, Addison-Wesley Publishing Company, 1973.

13. Viets, Hermann, "Directional Effects in 3-D Diffusers," AIAA Journal, Vol. 13, No. 6, June, 1975, pg. 823-825.

14. Meier, H.U., Michel, U. and Kreplin, H.P., "The Influence of Wind Tunnel Turbulence on the Boundary Layer Transition," International Symposium on Perspectives in Turbulent Studies, DFVLR Research Center, Gottingen, May 11-12, 1987, pp26-46.

15. Cebeci, T., and Smith, A. M. O., Analysis of Turbulent Boundary Layers, Acadenic Press, Inc., 1974.

16. Evans, R. L., "Freestream Turbulence Effects on Turbulent Boundary Layers in an Adverse Pressure Gradient," AIAA Journal, Vol 23, No.11, Nov., 1985, pp. 1814-1816.

17. Arnal, Daniel, "Influence De La Turbulence De L'Ecoulement General Sur Les Couches Limites Turbulentes En Fluide Incompressible," European Space Agency Technical Translation ESA TT - 411, September, 1977.

18. Coles, D., "The Law of the Wake in the Turbulent Boundary Layer," Journal of Fluid Mechanics, 1, Part 2, 1956.

19. White, F. M., Viscous Fluid Flow, McGraw-Hill, New York, 1974.

20. Das, D. K. and White, F. M., "Integral Skin Friction Prediction for Turbulent Separated Flows," ASME Journal of Fluids Engineering, Vol. 108, Dec., 1986.

21. Dean, R. B., "A Single Formula for the Complete Velocity Profile in a Turbulent Boundary Layer," ASME Journal of Fluids Engineering, Dec., 1976.

Table 1

Constants and Coefficients for Turbulence Decay

and

Integral Length Scale Equations

Condition	A	n	B	m
Test Section w/o Plate $0.50m < x' < 1.27m$	16.34	-1.79	2.26	0.105
$\alpha = 0°$, $X_o = 0.67m$ $1.23m < x' < 1.61m$	3.87	-1.542	1.276	0.229
$\alpha = 0°$, $X_o = 1.13m$ $1.69m < x' < 2.07m$	0.125	-0.897	0.394	0.552

NOTE: For equations 1 and 3, x' and λ_x have the units of cm.

Table 2a

Summary of Results

Condition	x (m)	U_∞ (m/s)	δ (cm)	θ (cm)	H_o	c_{f_o} x10^3	K	Re_θ	β
α = 0° LFST	0.56	27.2	1.47	0.156	1.410	3.33	0.998	2850	0
	0.94	27.0	2.01	0.229	1.420	2.99	0.965	4152	0
α = 2.6° LFST	0.56	29.9	1.68	0.201	1.455	2.87	1.047	4038	0.33
	0.94	28.4	2.77	0.338	1.443	2.44	0.990	6452	0.42
α = 5.2° LFST	0.56	32.6	2.36	0.297	1.431	2.63	1.051	6521	0.79
	0.94	30.3	3.45	0.462	1.480	2.12	1.009	9418	1.41

Table 2b

Summary of Results

Condition	x (m)	$\frac{\sqrt{u'^2}}{U_\infty}$ (%)	$\frac{\sqrt{v'^2}}{\sqrt{u'^2}}$	$\frac{\sqrt{w'^2}}{\sqrt{u'^2}}$	$\frac{\sqrt{q'^2}}{U_\infty}$ (%)	U_∞ (m/s)	L_x (cm)	λ_x (cm)	$\frac{\sqrt{u'^2}/U_\infty}{(Lx/\delta+2)}$
α = 0° X_o = 0.67m	0.56	4.83	1.10	1.27	5.45	26.3	3.84	5.48	0.0133
	0.94	3.92	1.17	1.38	4.68	26.1	4.09	6.09	0.0117
α = 2.6° X_o = 0.67m	0.56	4.67	1.09	1.05	4.88	29.2		5.37	
	0.94	4.23	0.86	0.90	3.90	27.6		5.92	
α = 5.2° X_o = 0.67m	0.56	4.63	1.23	1.06	5.10	32.4		5.15	
	0.94	4.16	1.03	1.02	4.29	29.5		5.84	
α = 0° X_o = 1.13m	0.56	3.55	1.10	1.27	4.00	25.7	6.69	6.20	0.0072
	0.94	3.24	0.94	1.16	3.37	25.6	7.49	6.47	0.0071
α = 2.6° X_o = 1.13m	0.56	3.38	1.32	1.14	3.92	29.7		5.96	
	0.94	3.11	1.19	1.13	3.45	27.7		6.22	
α = 5.2° X_o = 1.13m	0.56	3.19	1.35	1.18	3.78	32.5		5.98	
	0.94	3.13	1.28	1.10	3.55	29.8		6.05	

Table 2c

Summary of Results

Condition	x (m)	δ (cm)	θ (cm)	H	c_f x10^3	$\frac{U_\infty \theta}{\nu}$	$\frac{\sqrt{\overline{q'^2}}/U_\infty}{\lambda_x/\delta}$ (%)	$-\frac{\Delta H}{H_o}$	$\frac{\Delta c_f}{c_{fo}}$
α = 0° X_o = 0.67m	0.56	2.36	0.146	1.326	3.93	2582	2.35	0.067	0.164
	0.94	3.00	0.219	1.322	3.50	3972	2.31	0.072	0.164
α = 2.6° X_o = 0.67m	0.56	3.15	0.208	1.318	3.52	4082	2.86	0.094	0.230
	0.94	4.90	0.333	1.302	3.13	6185	3.23	0.096	0.261
α = 5.2° X_o = 0.67m	0.56	3.75	0.298	1.302	3.19	6499	3.71	0.090	0.211
	0.94	5.50	0.458	1.305	2.80	9108	4.04	0.114	0.295
α = 0° X_o = 1.13m	0.56	2.26	0.155	1.347	3.73	2718	1.46	0.047	0.112
	0.94	2.95	0.224	1.343	3.39	3978	1.53	0.057	0.127
α = 2.6° X_o = 1.13m	0.56	3.23	0.211	1.310	3.38	4207	2.12	0.100	0.191
	0.94	4.58	0.348	1.321	2.97	6478	2.54	0.085	0.219
α = 5.2° X_o = 1.13m	0.56	3.82	0.292	1.311	2.99	6380	2.41	0.083	0.125
	0.94	5.55	0.467	1.324	2.64	9352	3.26	0.105	0.240

Table 2d

Summary of Results

Condition	x (m)	c_{fo} x10^3	H_o	β
α = 0° X_o = 0.67m	0.56	3.377	1.418	0
	0.94	3.008	1.424	0
α = 2.6° X_o = 0.67m	0.56	2.861	1.455	0.26
	0.94	2.482	1.440	0.43
α = 5.2° X_o = 0.67m	0.56	2.634	1.431	0.60
	0.94	2.162	1.474	0.94
α = 0° X_o = 1.13m	0.56	3.353	1.414	0
	0.94	3.007	1.424	0
α = 2.6° X_o = 1.13m	0.56	2.837	1.455	0.27
	0.94	2.436	1.443	0.48
α = 5.2° X_o = 1.13m	0.56	2.657	1.429	0.65
	0.94	2.129	1.479	1.03

APPENDIX

Velocity Profile Correlation

The velocity profiles of the boundary layers were found to fit a formula suggested by Hancock (2) and Dean (21), equation 9.

$$u/u_* = 2.439 \ln u_* y/\nu + 5.2 + 2.439[(1 + 6\Pi)(y/\delta)^2 - (1 + 4\Pi)(y/\delta)^3]$$

Eqn. 9

The first two terms of eqn. 9 represent the law of the wall, equation 4, whereas the last term represents the deviation from the law of the wall (the wake function) and becomes significant in the wake region of the boundary layers. In this appendix, values of Π, the wake parameter, are correlated with β and free-stream turbulence parameters. The velocity profiles obtained were found to fit eqn. 9 reasonable well for both positive and negative values of Π, whereas they did not fit Coles' wake function ($2 \sin^2 (\pi/2) (y/\delta)$) well for negative values of Π.

a) For the case of $\beta = 0$ and low free-stream turbulence, the values of Π fit the results presented by Cebeci (15) reasonably well, as shown in Fig. 20.

b) For the case of $\beta = 0$ and with free-stream turbulence, the results of Hancock (2) and the present results, presented in Fig. 21, show that Π is a strong function of the free-stream turbulence parameter, $\sqrt{u'^2}/U_\infty / ((L_x / \delta) + 2)$.

c) For the case of $\beta > 0$, values of Π are shown to be a strong function of β (see Fig. 22). The results of this study with low free-stream turbulence fit the results presented by White (19) $\Pi = 0.8 (0.5 + \beta)^{0.75}$ and Das (20) for equilibrium boundary layers reasonably well.

d) For the case of $\beta > 0$ and with free-stream turbulence, the results obtained by Evans (16) along with the present results form a distinct separate curve which parallels the curves obtained by White (19) and Das (20). The results of Arnal (17), both with and without free-stream turbulence, do not fit any of the curves presented. These results then suggest that Π is a function of both β and a free-stream turbulence parameter. A reasonably good correlation of these parameters is presented in Fig. 23. More data needs to be obtained to better define the curves in this graph, and to obtain this correlation for larger values of β.

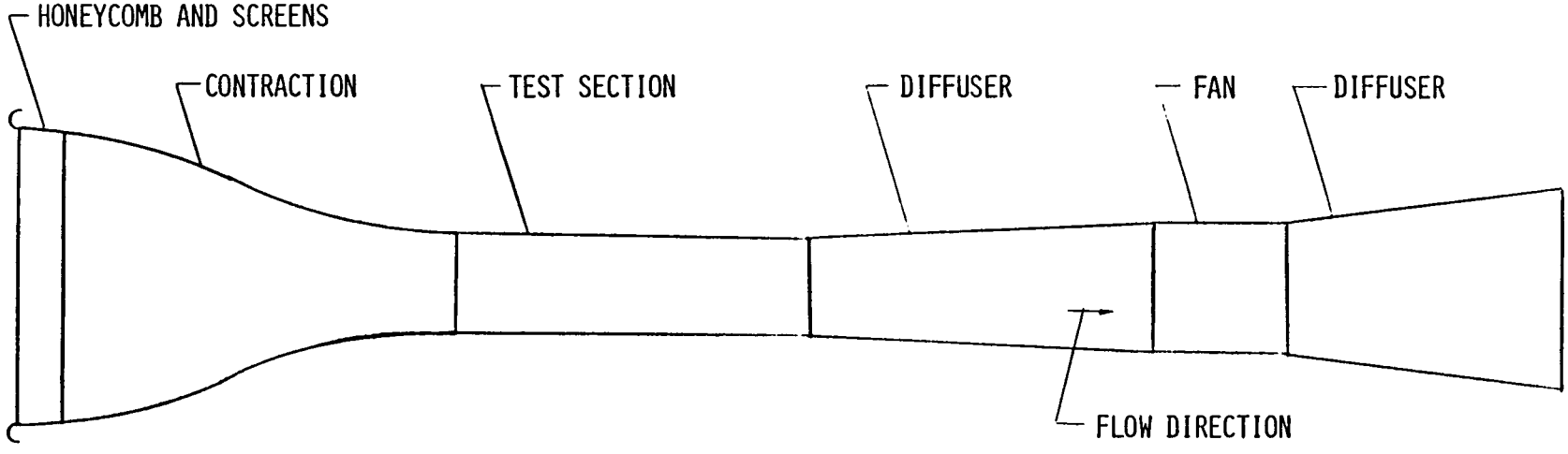

Fig. 1

Cal Poly 0.88m x 1.18m Wind Tunnel

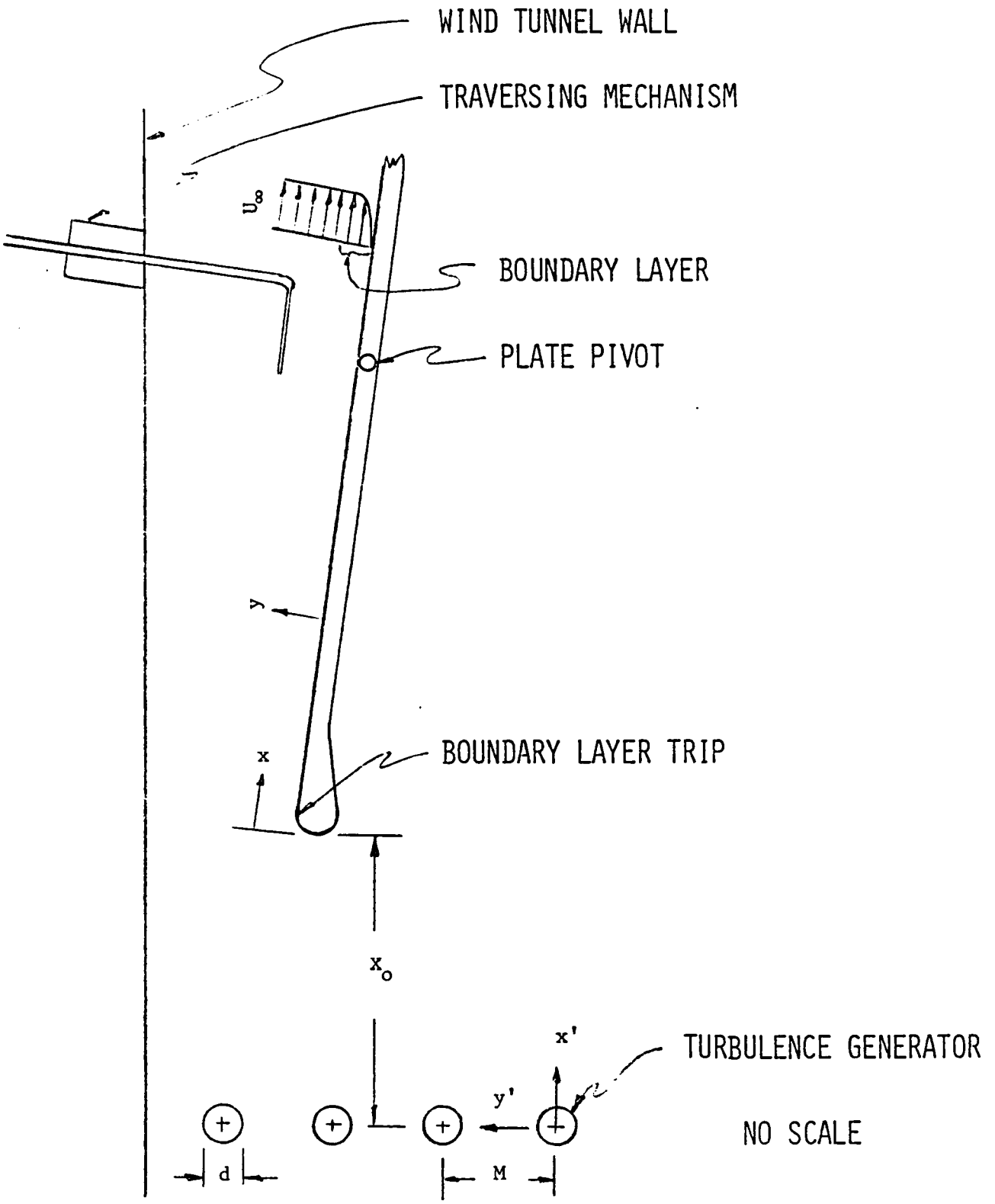

Fig. 2

Flat Plate and Turbulence Generator

Fig. 3

Average (E) and RMS ($\sqrt{e'^2}$)
voltage outputs of a hot wire
downstream of rod set.
x'/M = 0.38
Wire calibration: 1 volt = 13.3 m/s

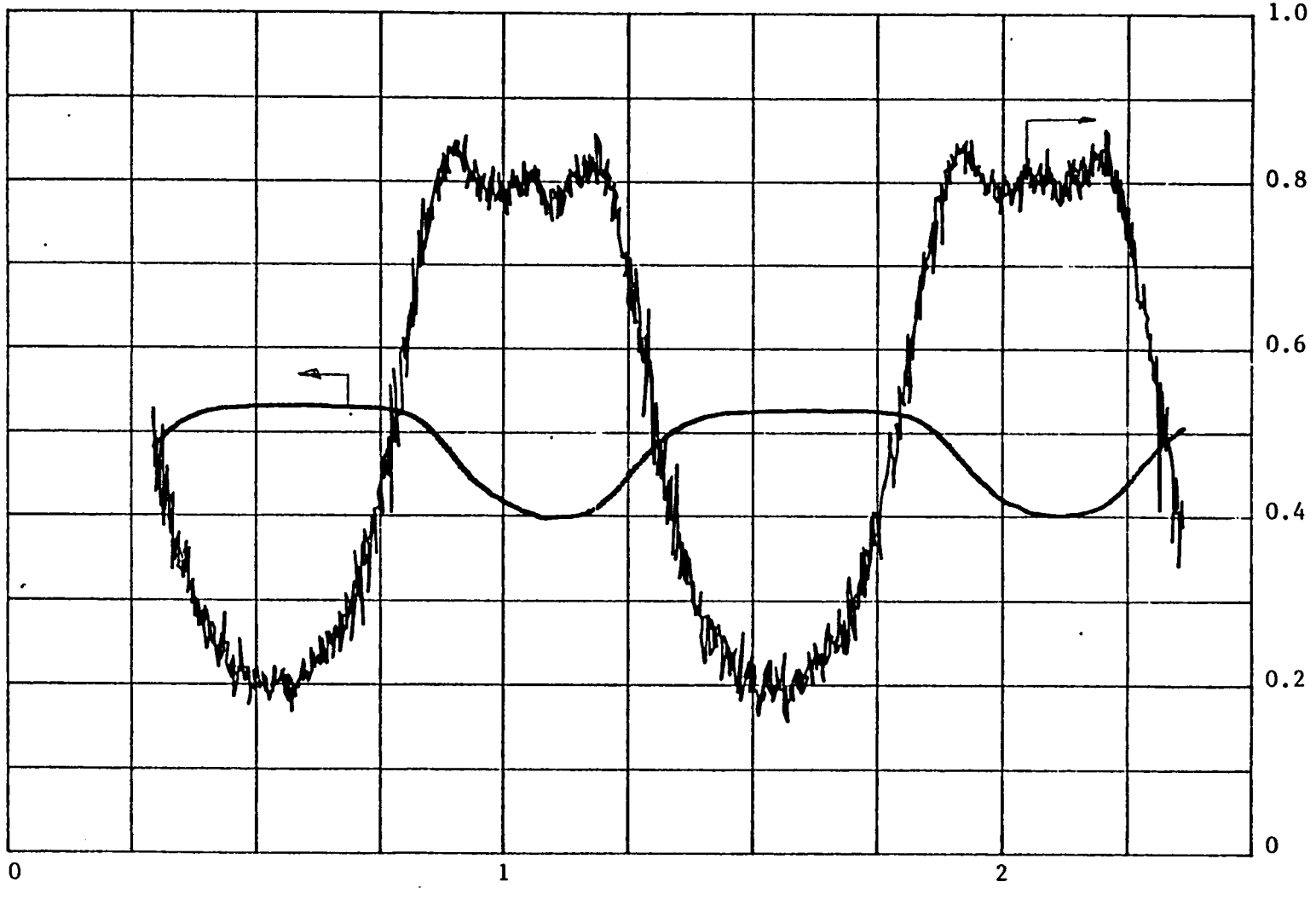

Fig. 4

Average (E) and RMS ($\sqrt{e'^2}$)
voltage outputs of a hot wire
downstream of a rod set.
x'/M = 0.86
Wire calibration: 1 volt = 13.3 m/s

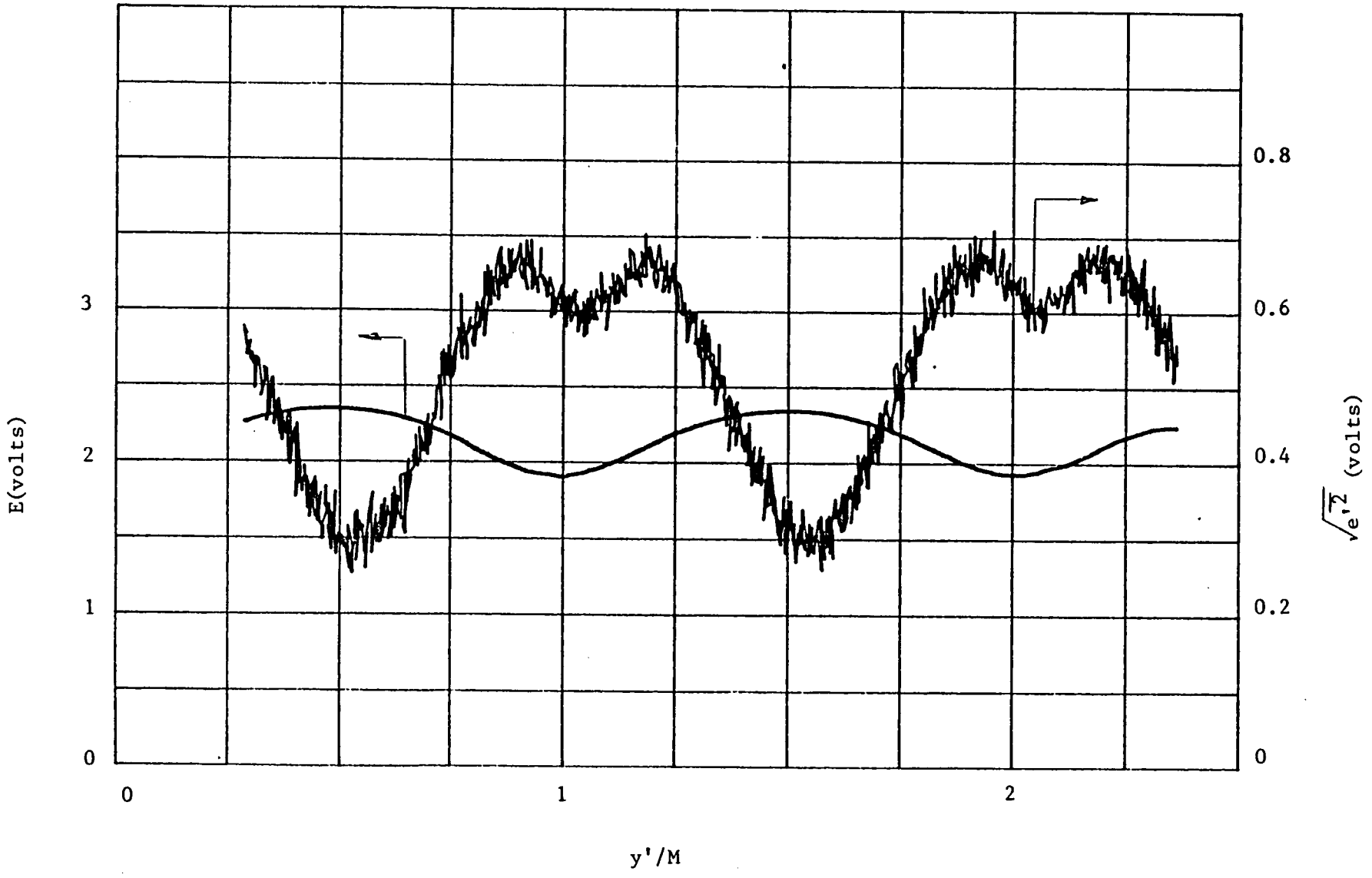

Fig. 5

Average (E) and RMS ($\sqrt{e'^2}$)
voltage outputs of a hot wire
downstream of a rod set.
x'/M = 1.62
Wire calibration: 1 volt = 13.3 m/s

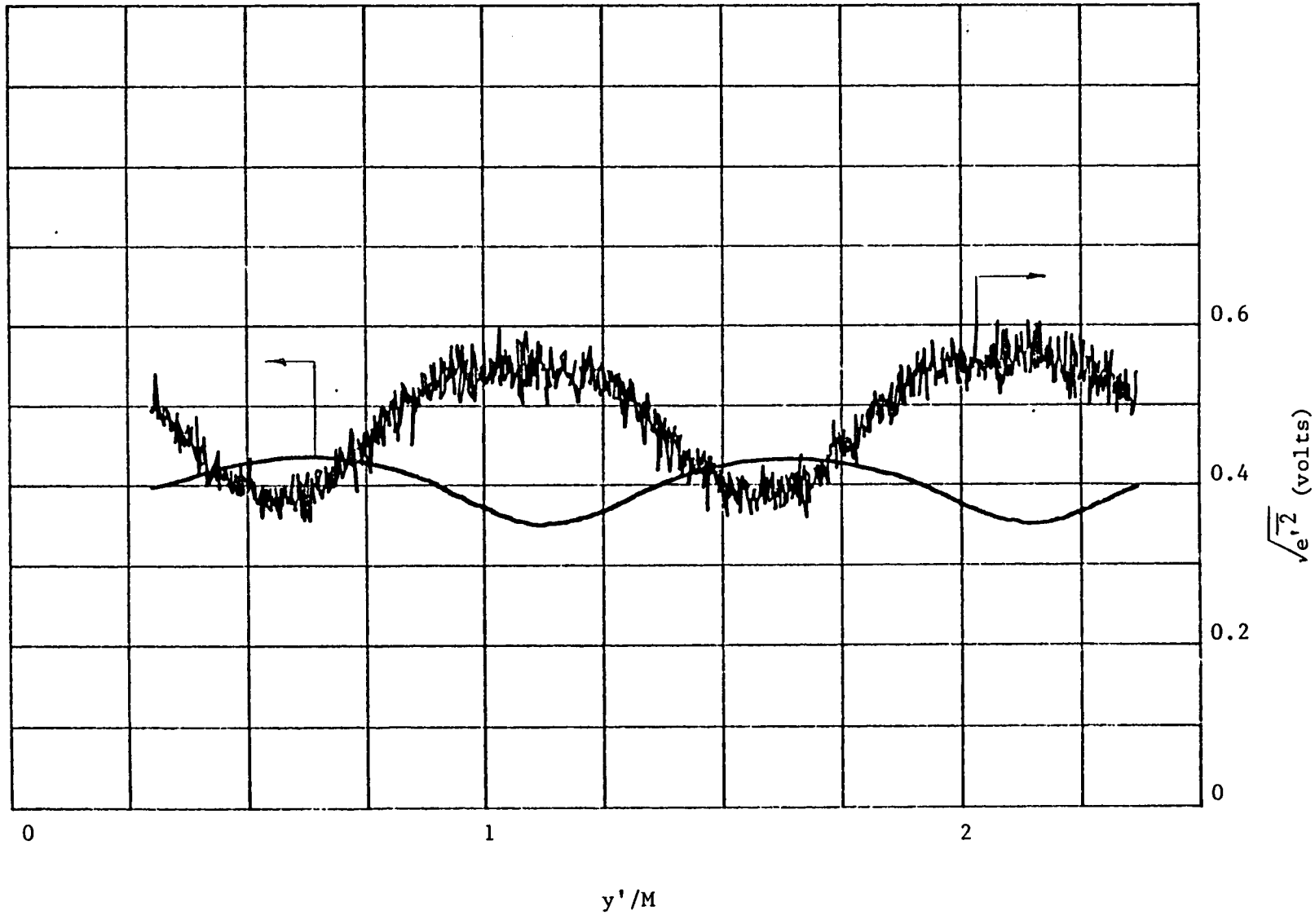

Fig. 6

Average (E) and RMS ($\sqrt{e'^2}$)
voltage outputs of a hot wire
downstream of a rod set.
x'/M = 3.14
Wire calibration: 1 volt = 13.3 m/s

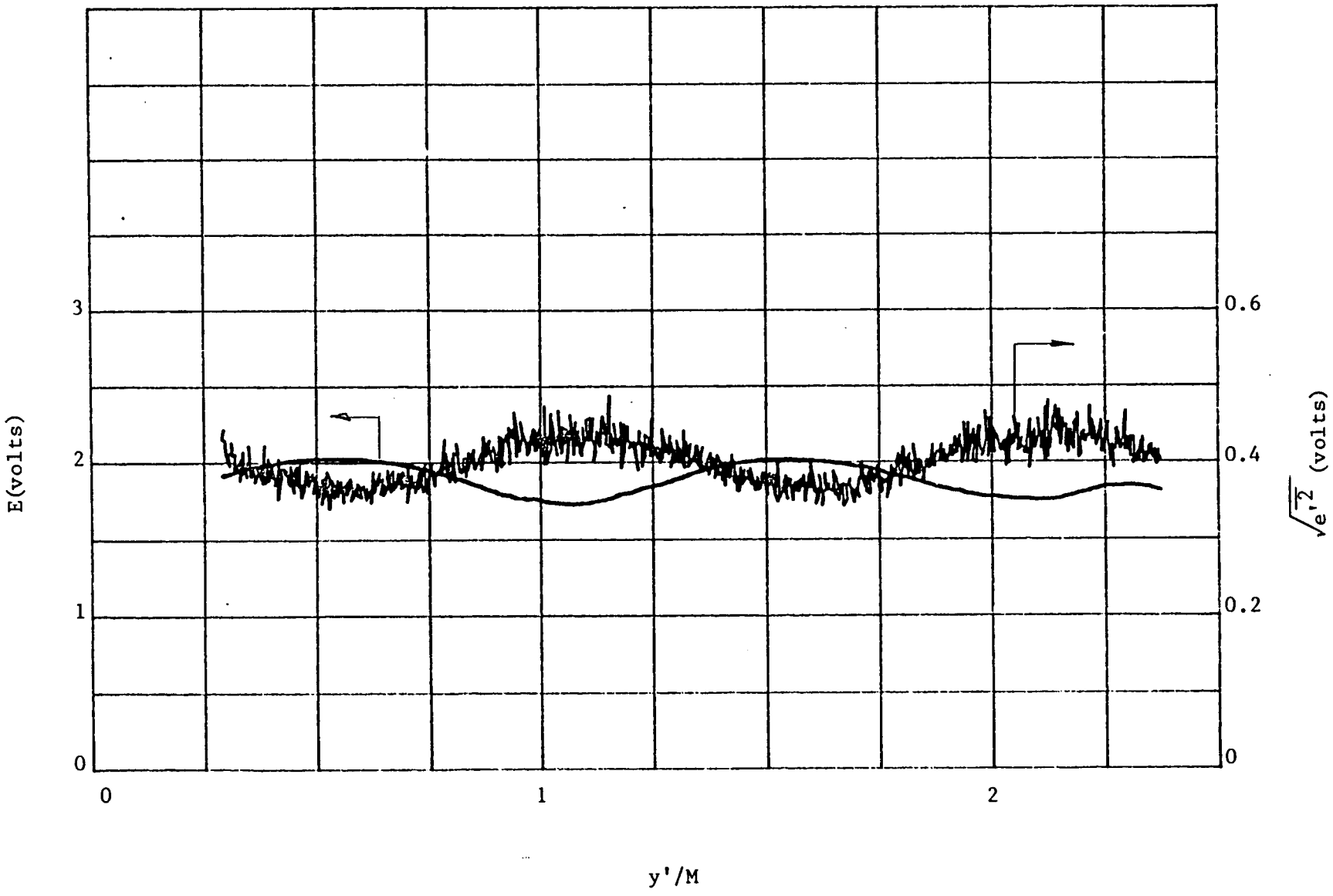

Fig. 7

Average (E) and RMS ($\sqrt{e'^2}$)
voltage outputs of a hot wire
downstream of a rod set.
x'/M = 4.33
Wire calibration: 1 volt = 13.3 m/s

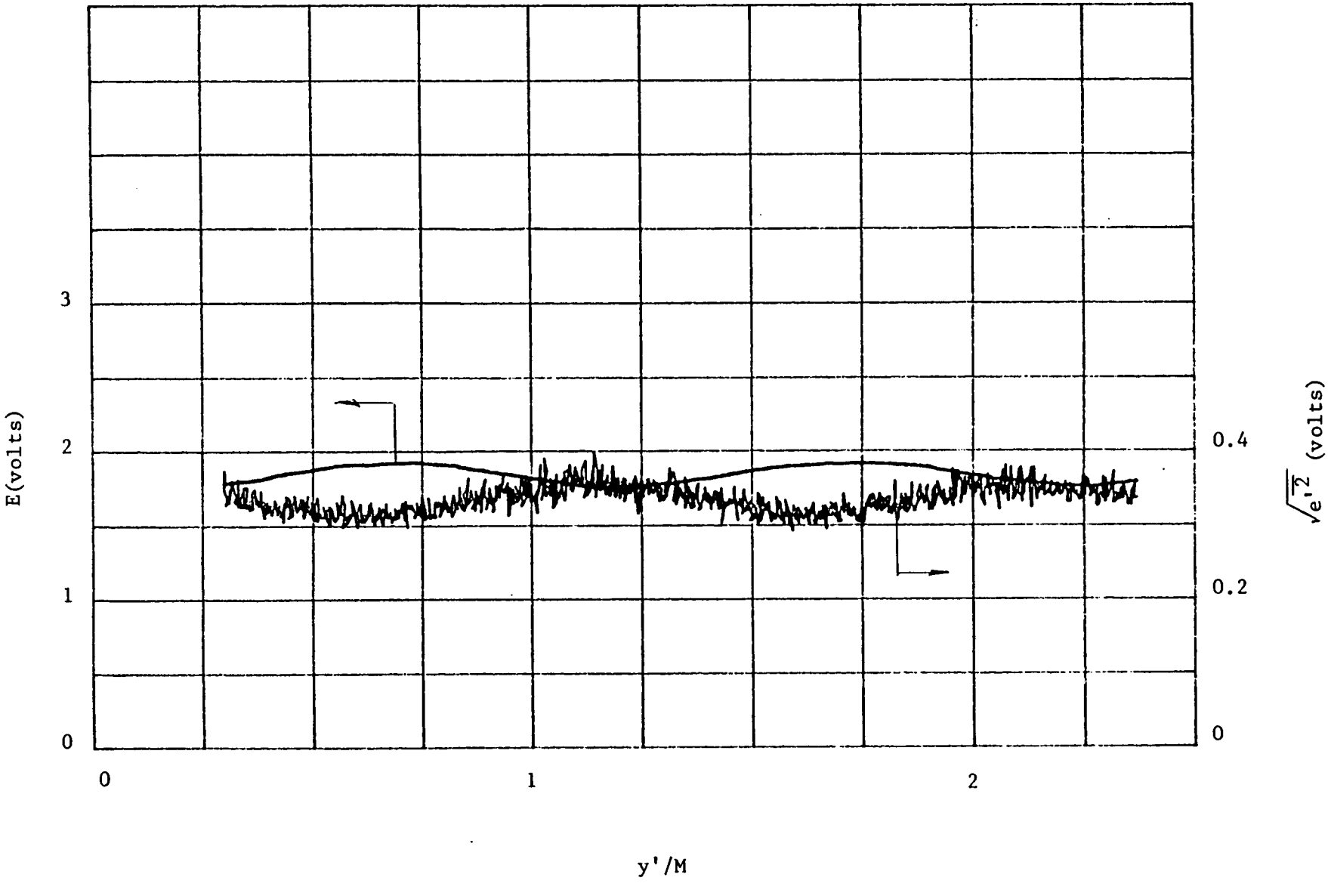

Fig. 8

Average (E) and RMS ($\sqrt{e'^2}$)
voltage outputs of a hot wire
downstream of a rod set.
x'/M = 7.90
Wire calibration: 1 volt = 13.3 m/s

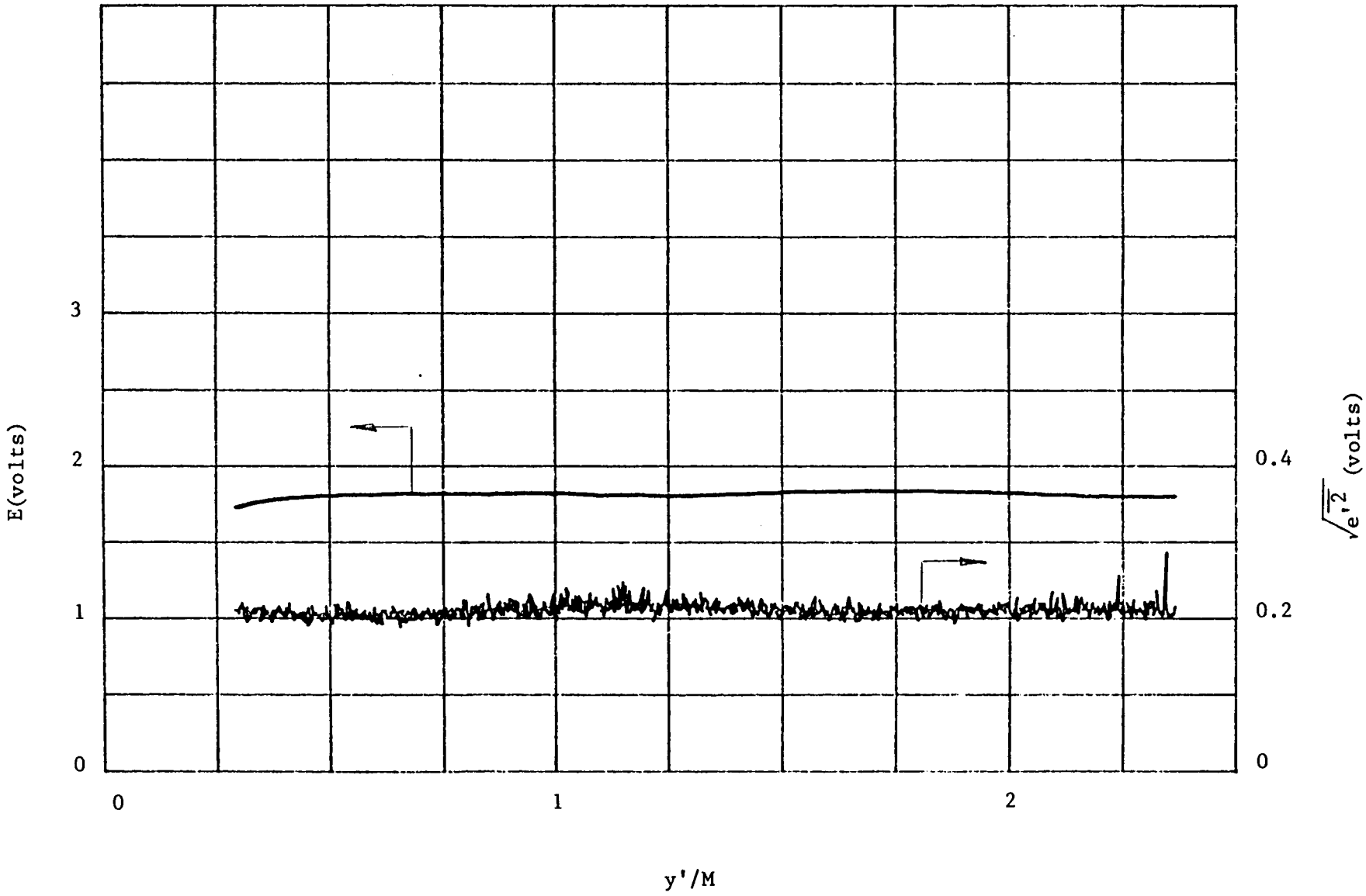

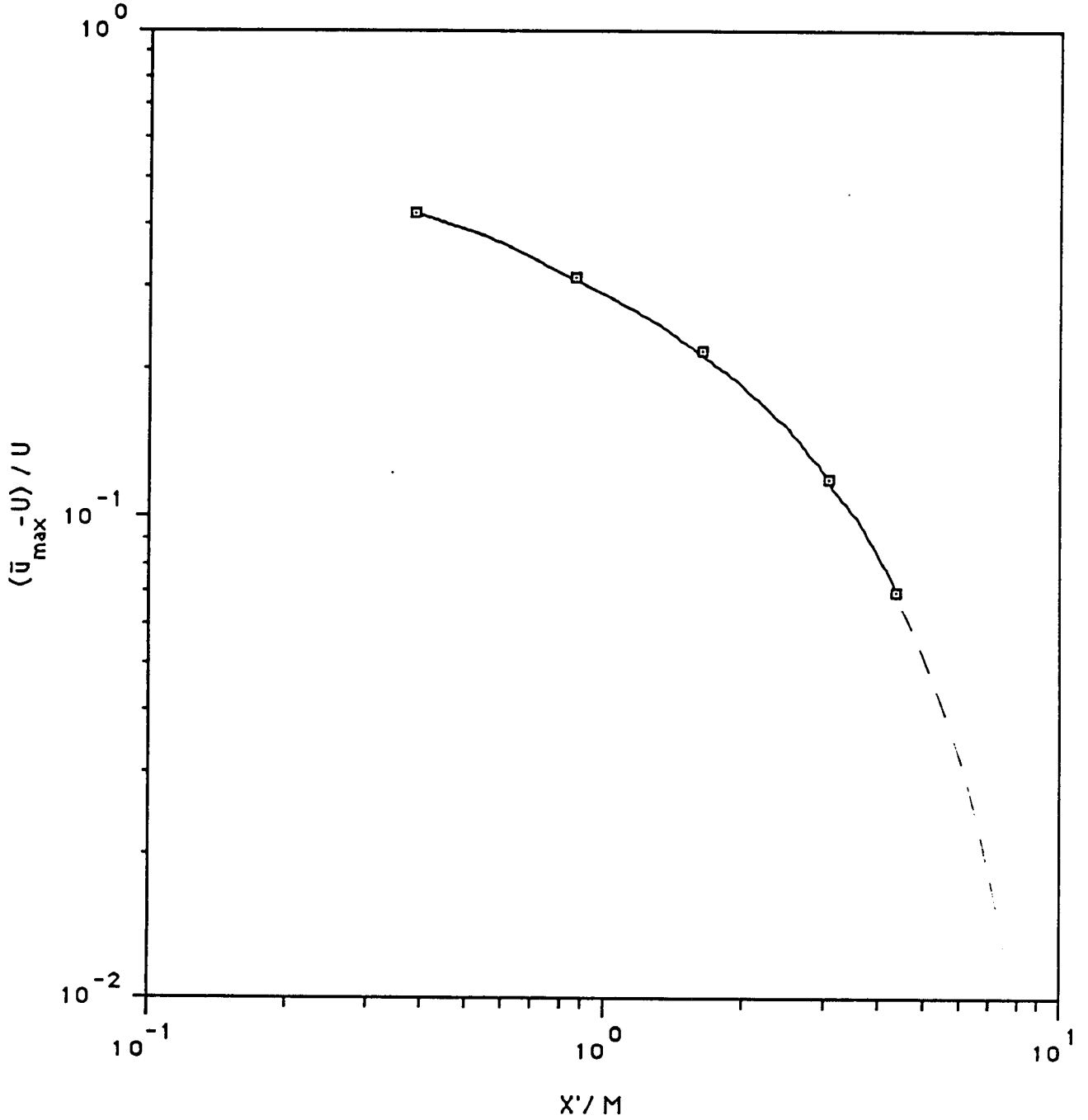

FIG. 9

Flow nonuniformity downstream of rods

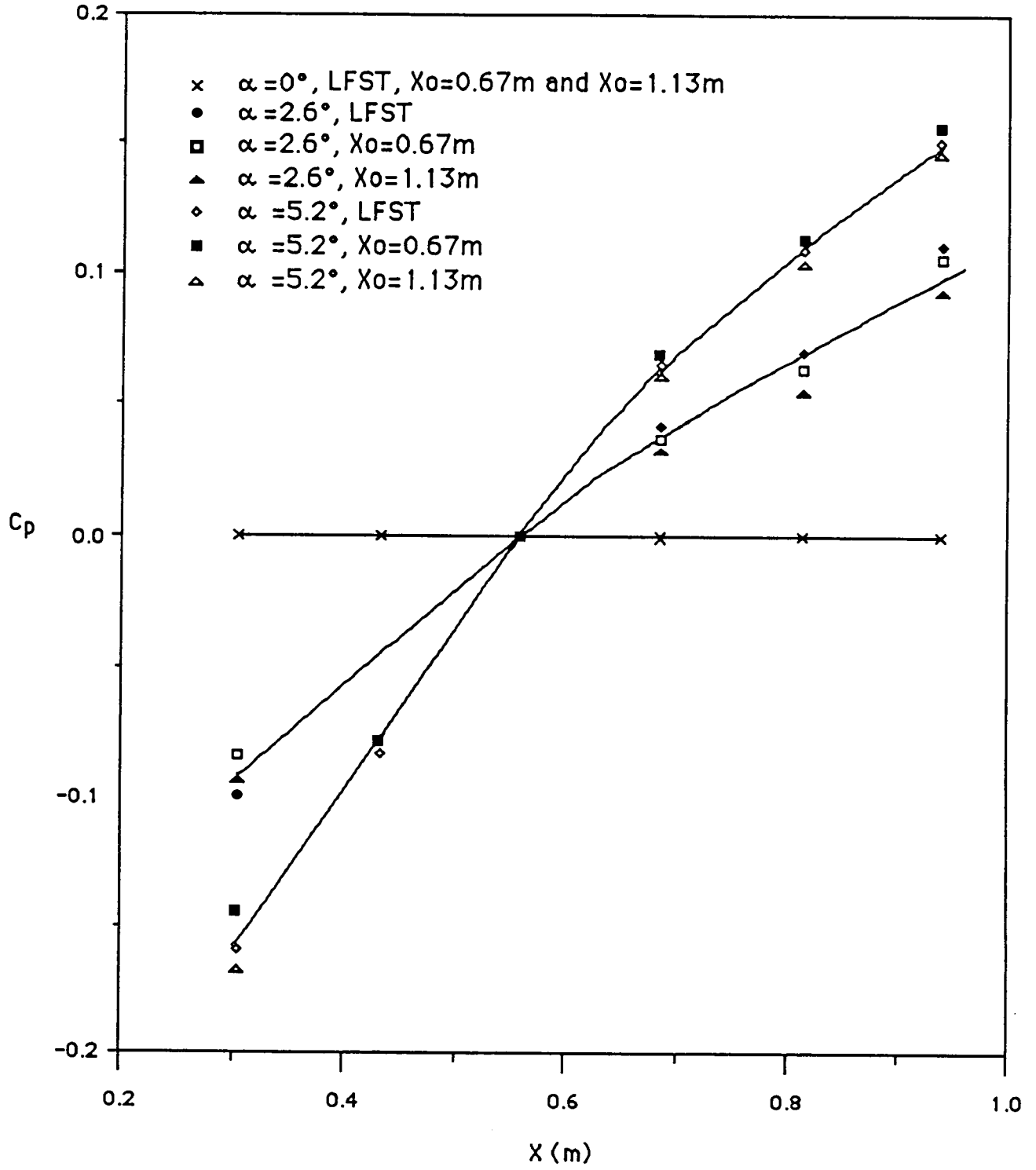

FIG. 10

Plate static pressure coefficient along plate

ORIGINAL PAGE IS
OF POOR QUALITY

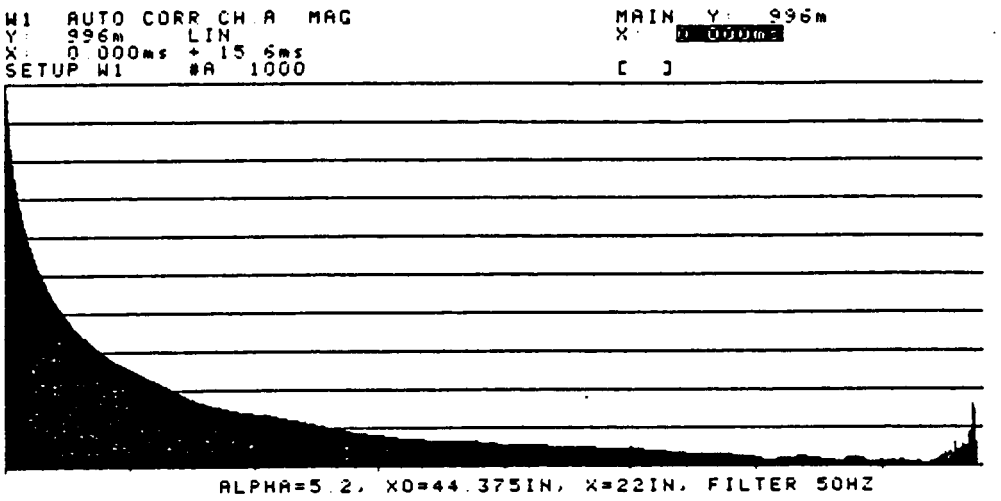

$\alpha = 5.2^{o}$, $X_o = 1.13m$, $x = 0.56m$

Fig. 11

Autocorrelation Coefficient vs. Δt

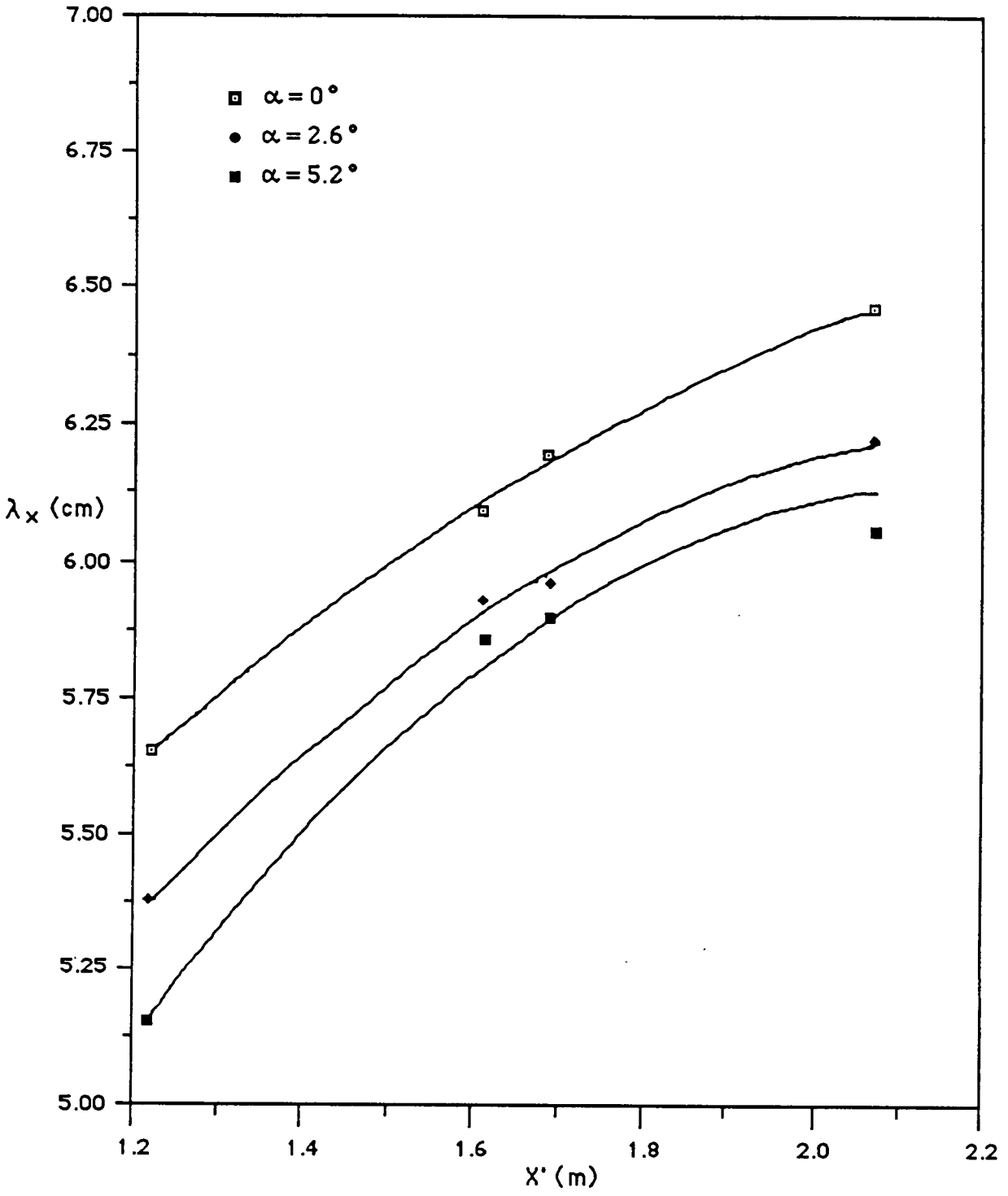

FIG. 12

Integral scale of turbulence vs. distance downstream of rods

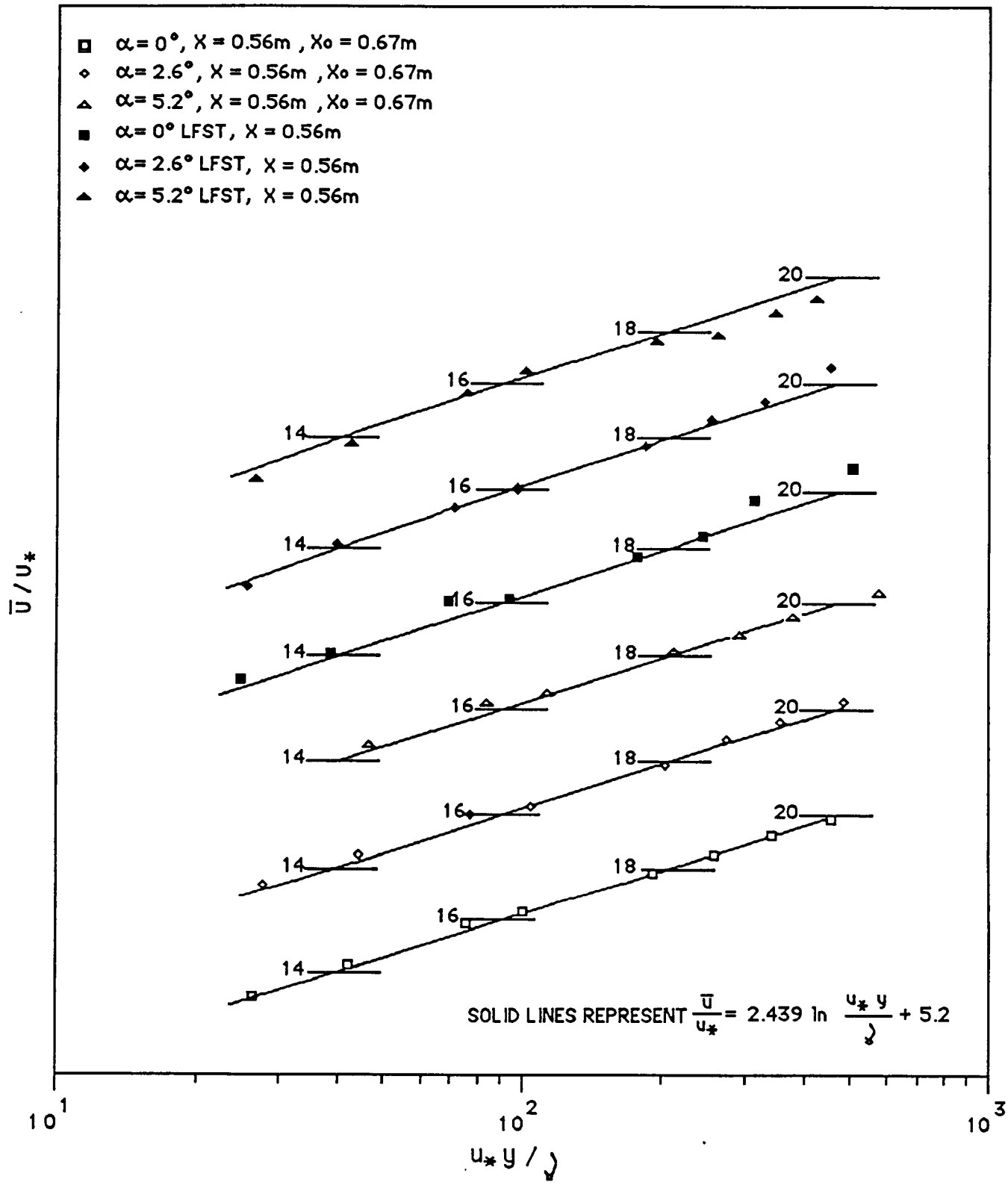

FIG. 13

Velocity profiles in logarithmic law of the wall region

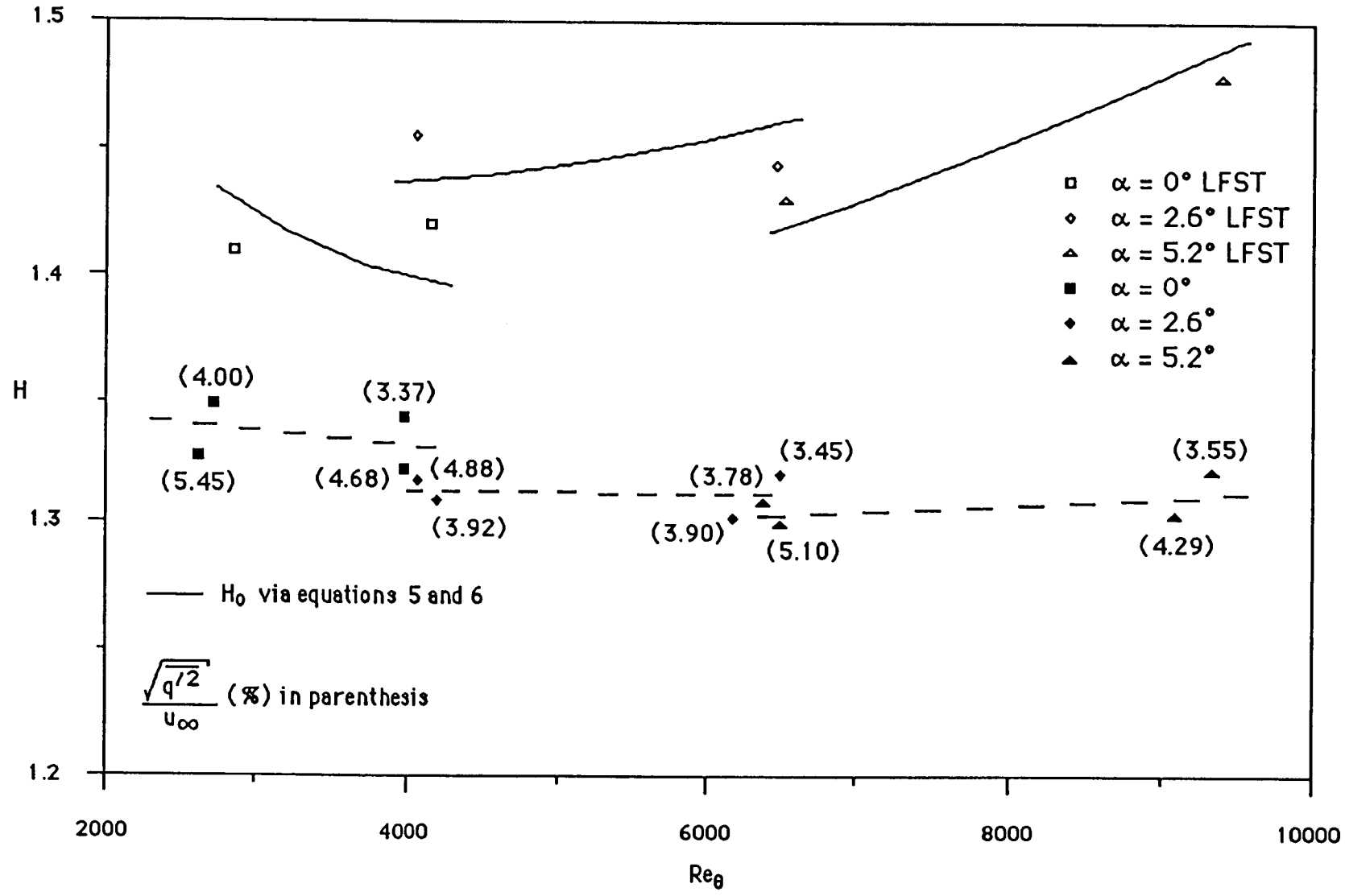

FIG. 14
Boundary layer shape factor vs. Reynolds number

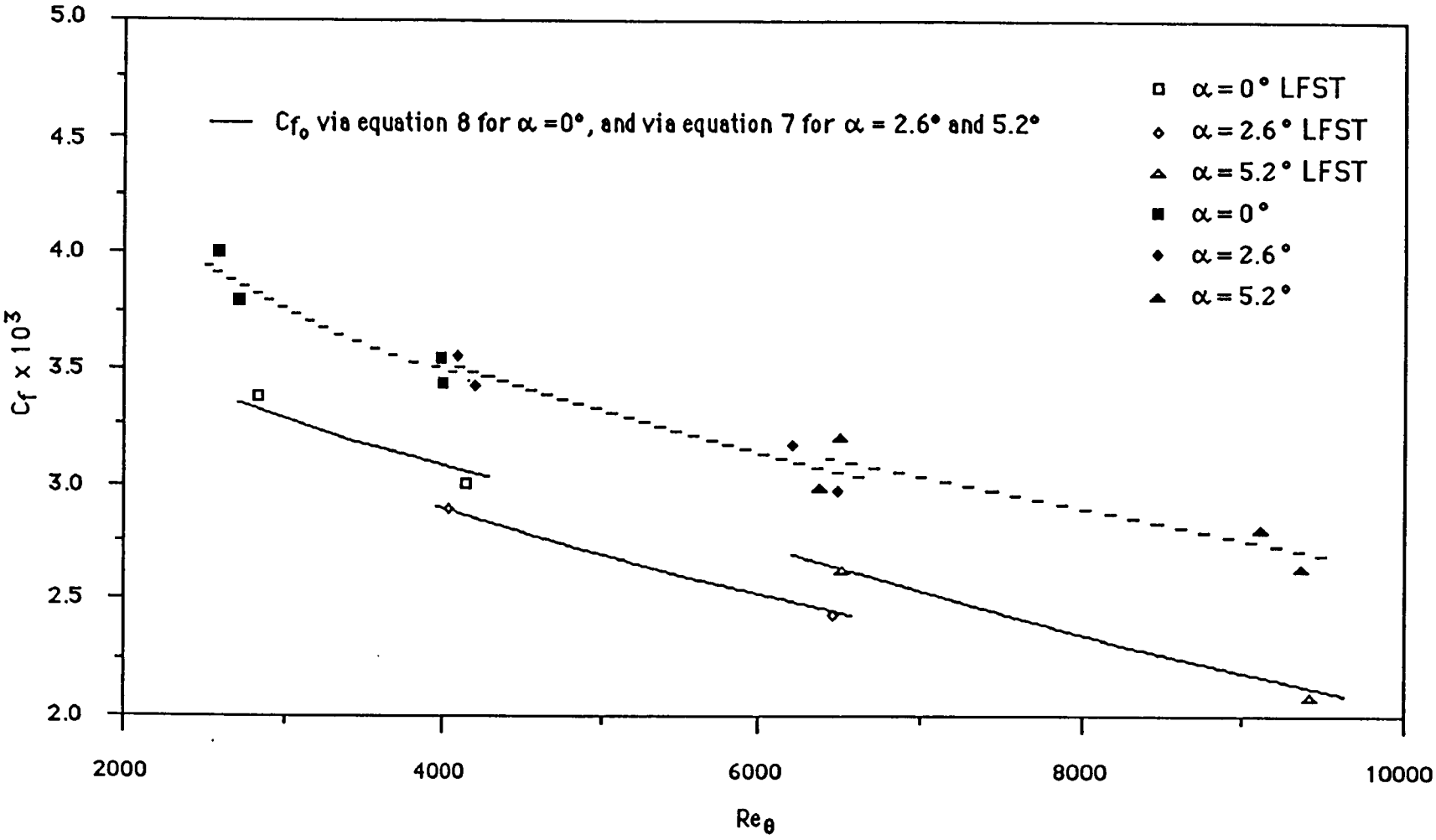

FIG. 15

Boundary layer skin friction coefficient vs. Reynolds number

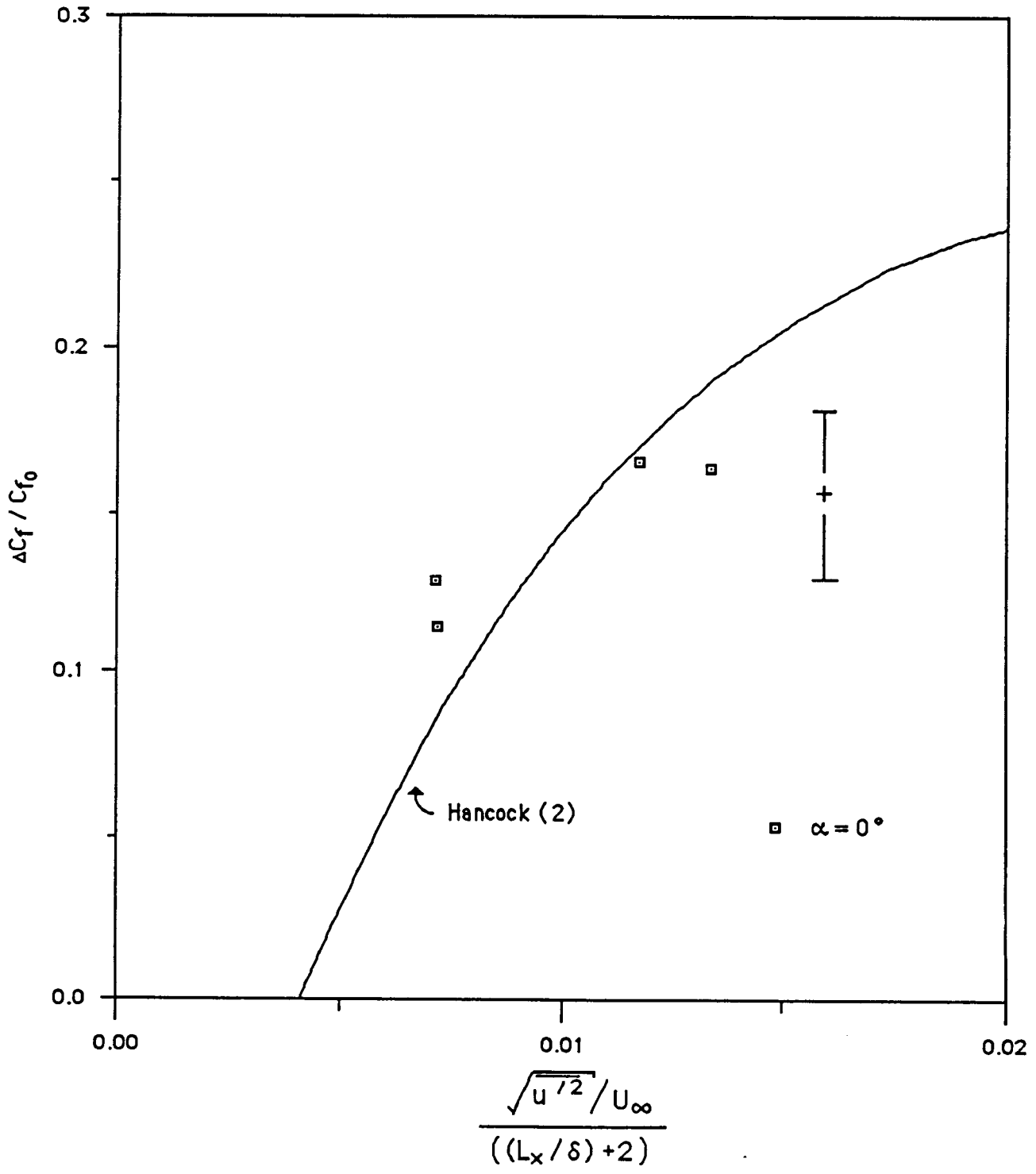

FIG. 16

Fractional change of skin friction vs. Hancock's free-stream turbulence parameter

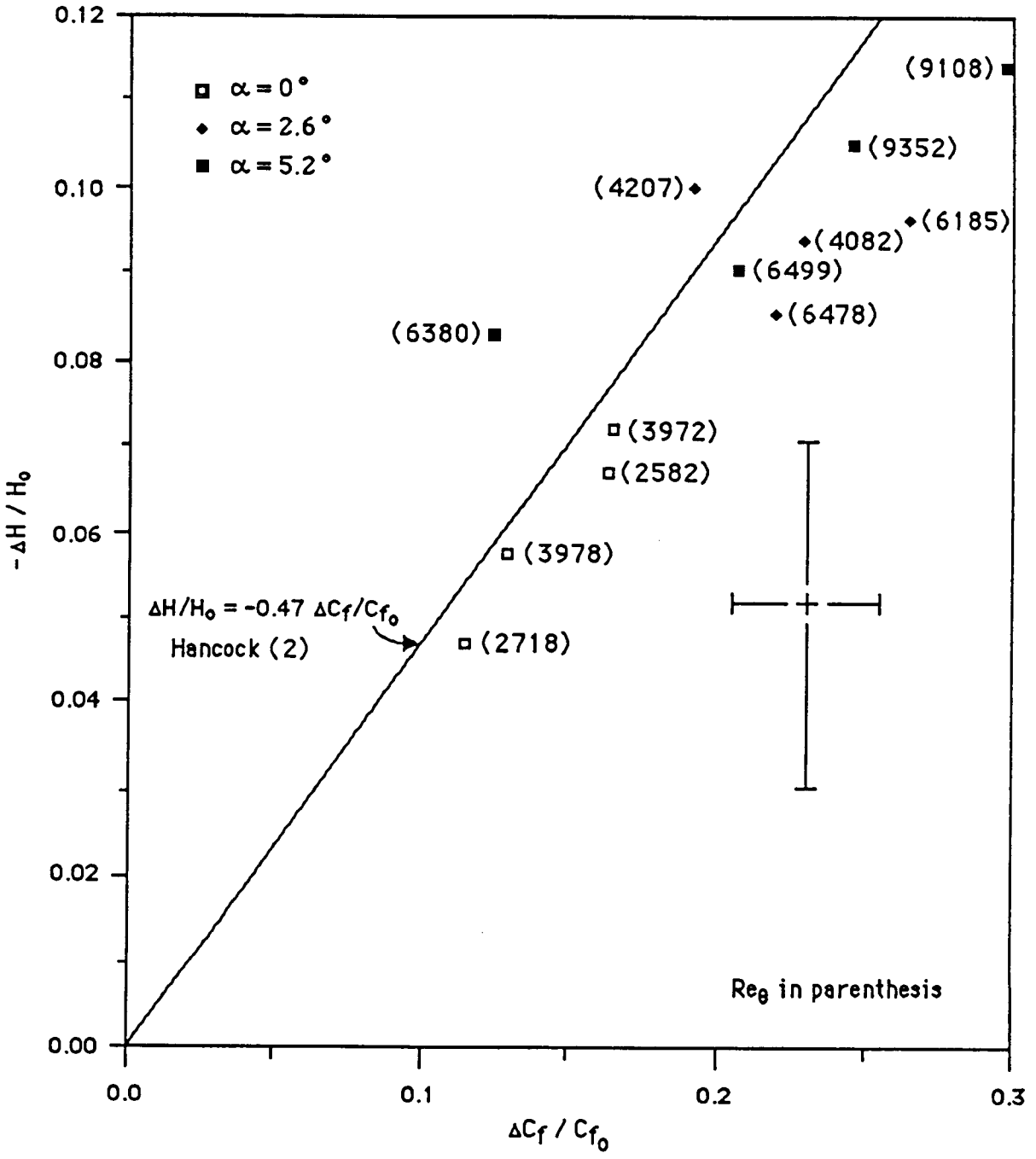

FIG. 17

Fractional change in skin friction vs. fractional change in shape factor

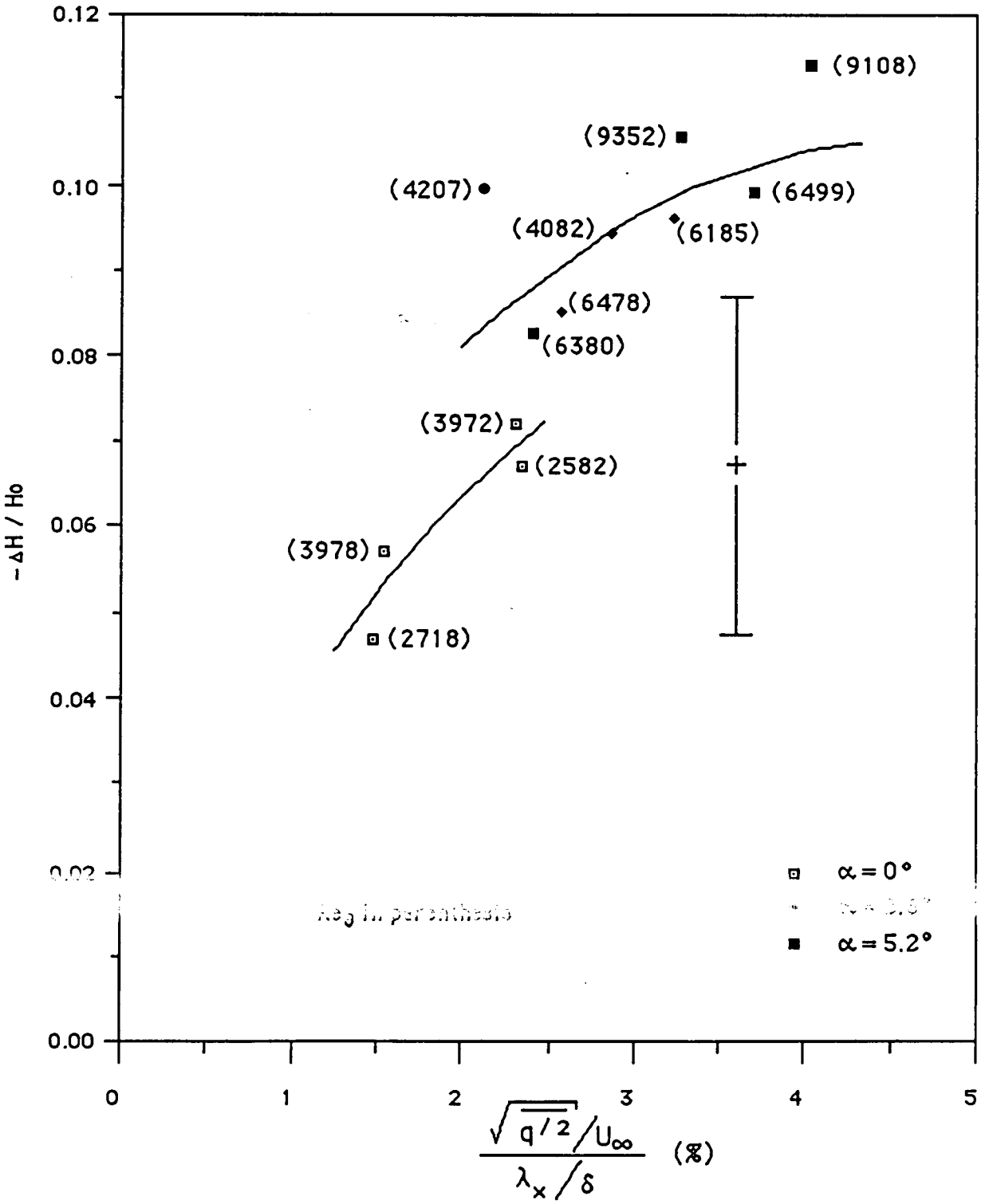

FIG. 18

Fractional change in shape factor vs. free-stream turbulence parameter

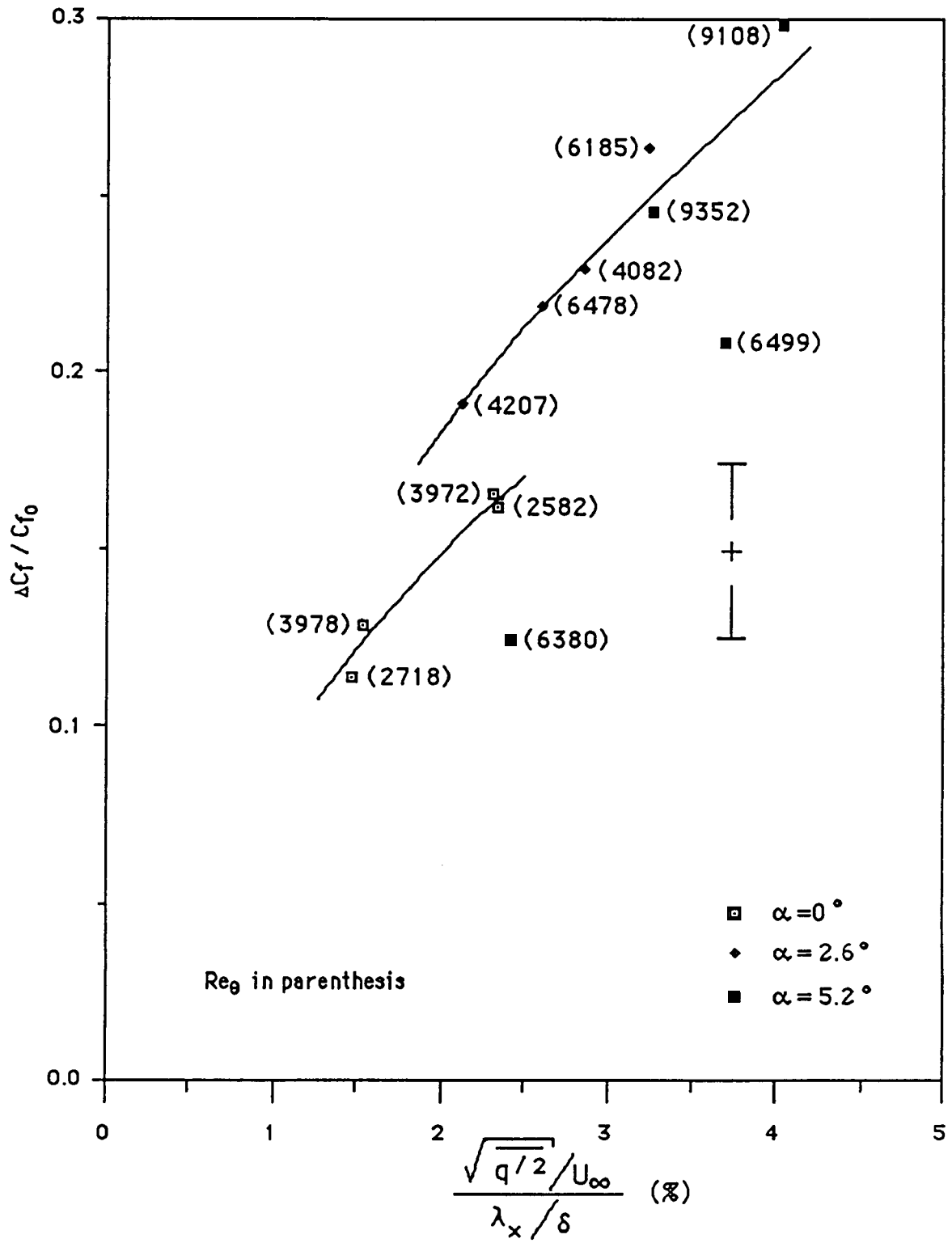

FIG. 19

Fractional change in skin friction vs. free-stream turbulence parameter

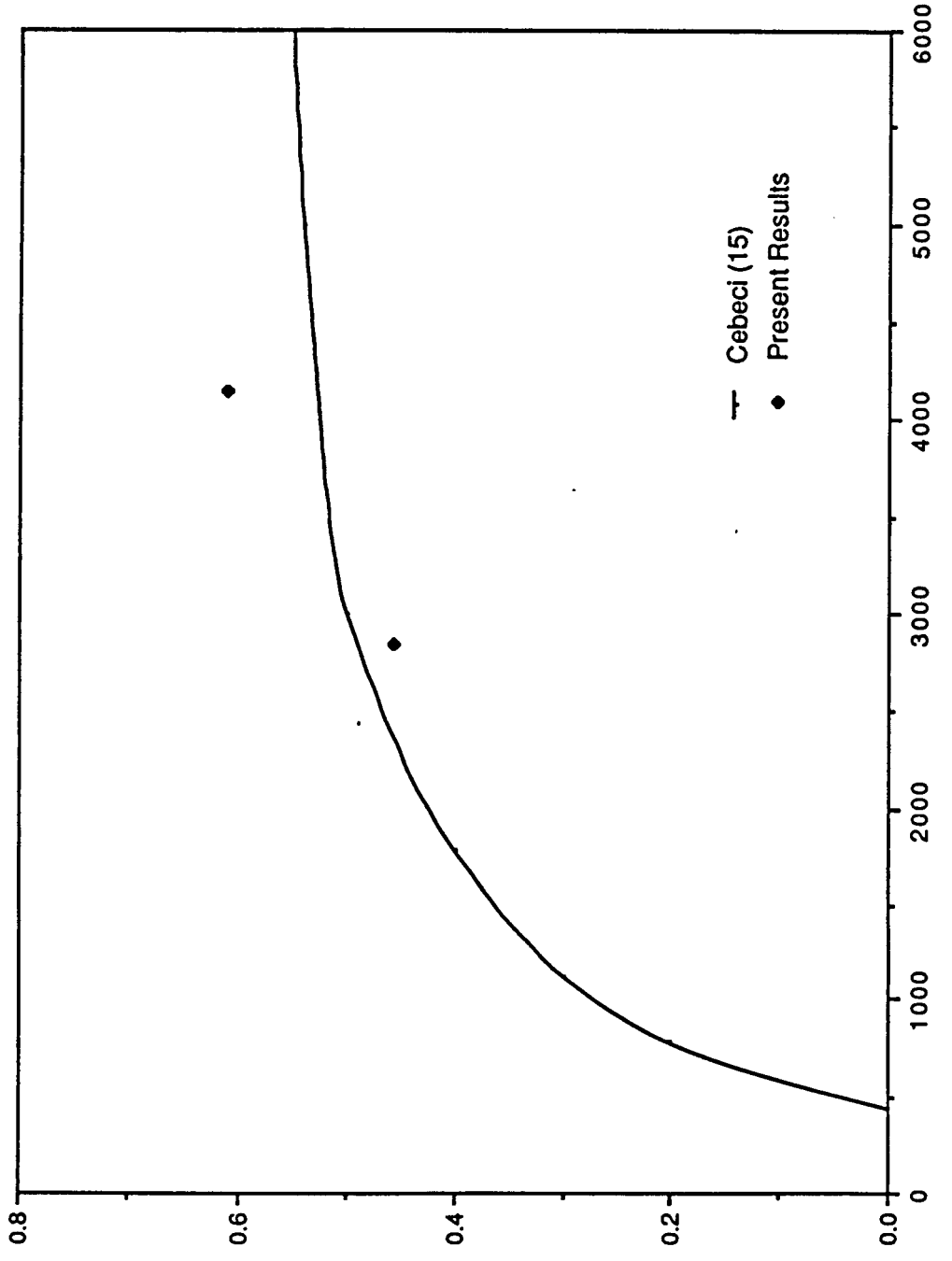

Fig. 20 Variation of wake parameter with momentum thickness Reynolds number for $\beta = 0°$ and LFST.

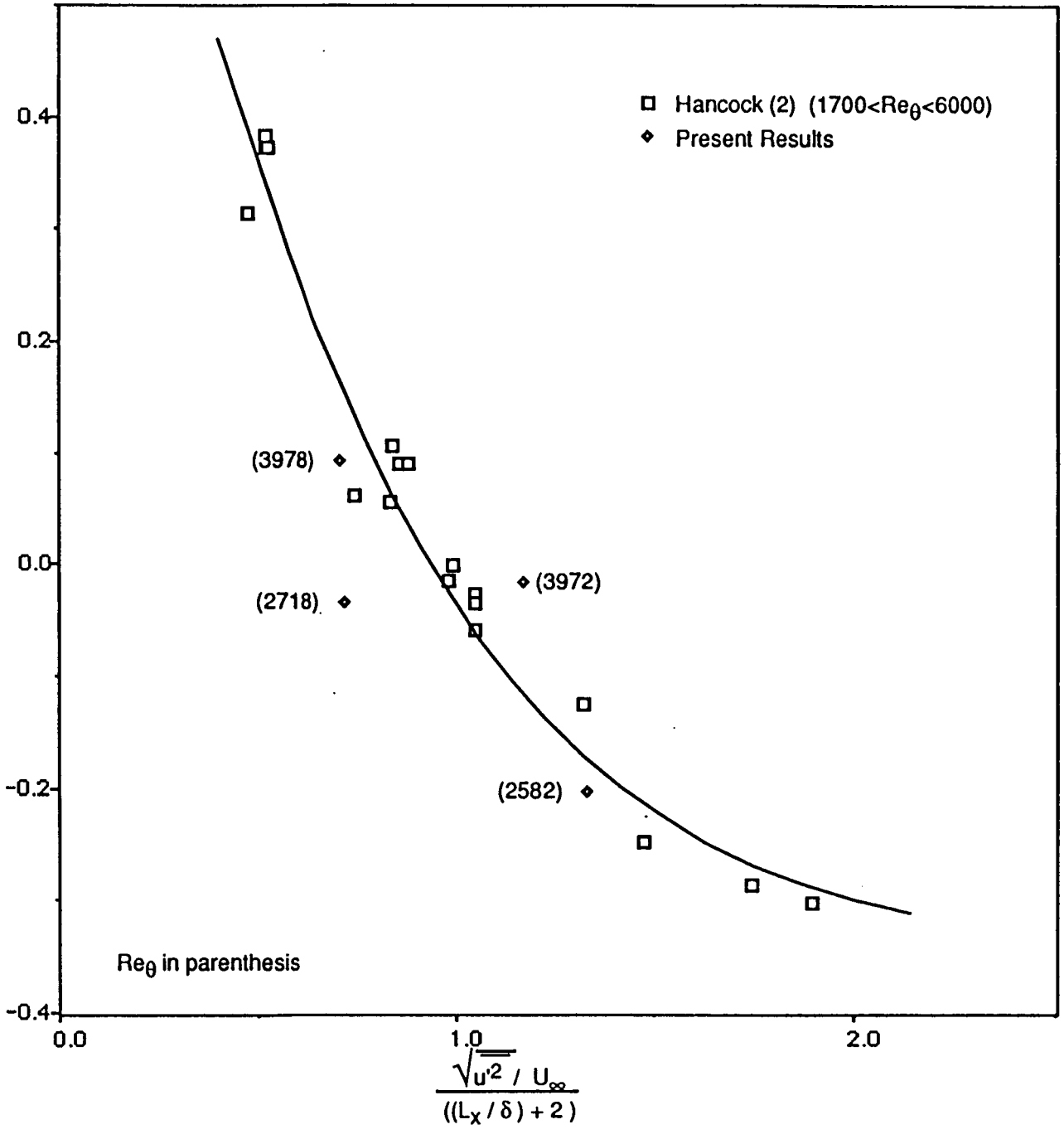

Fig. 21 Wake parameter as a function of a free-stream turbulence parameter for $\beta = 0$

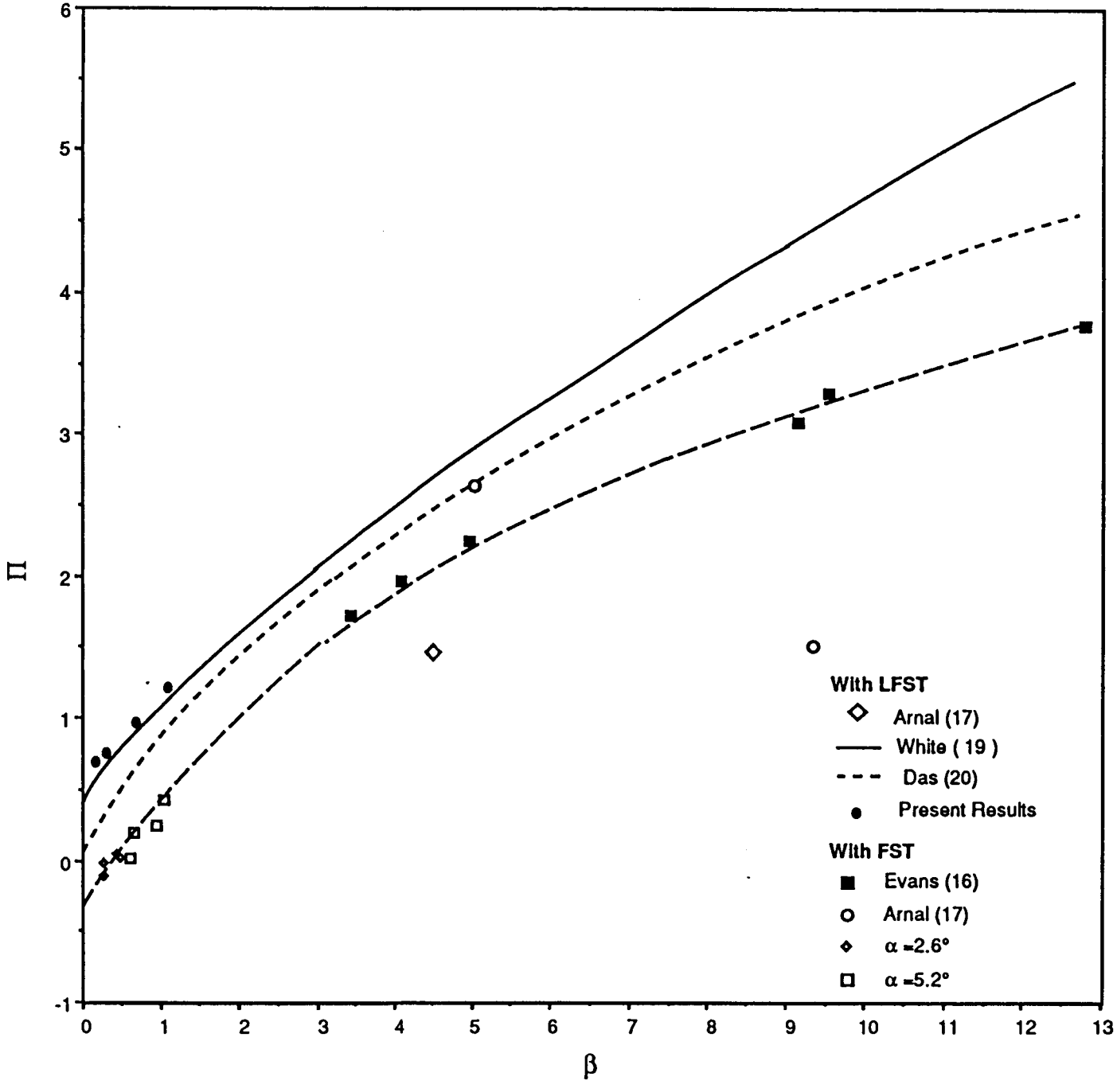

Fig. 22 Wake parameter versus β for β > 0.

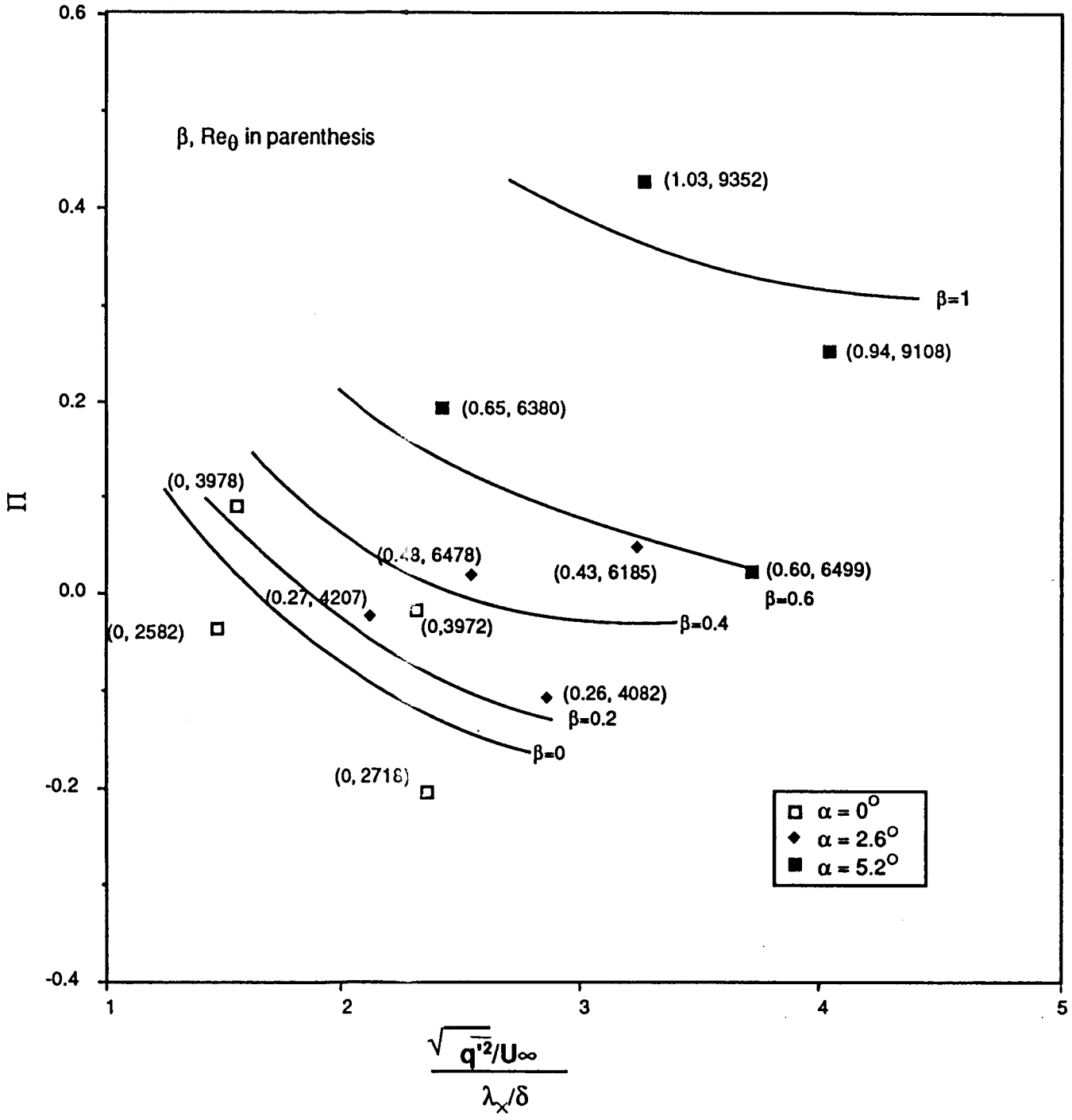

Fig. 23 Wake parameter as a function of turbulence intensity for constant β